

# STELLAR ANGULAR DIAMETERS FROM LUNAR OCCULTATIONS

Richard Allen Berg

St. Louis, Missouri

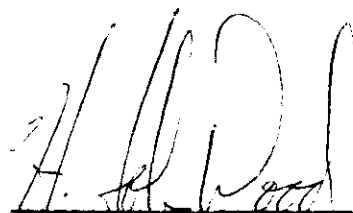
A Dissertation Presented to  
the Graduate Faculty of the  
University of Virginia  
in Candidacy for the Degree of Doctor of Philosophy

Leander McCormick Observatory  
University of Virginia

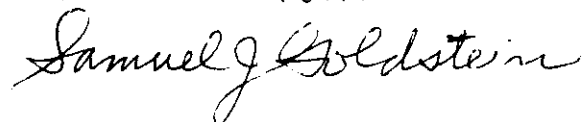
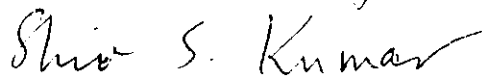
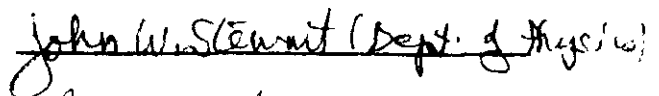
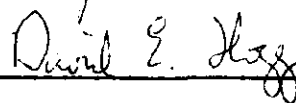
December  
1969

CORRECTIONS

Accepted by the Faculty of the Astronomy Department,  
University of Virginia, in partial fulfillment of the  
degree, Doctor of Philosophy



Director of Dissertation



STELLAR ANGULAR DIAMETERS FROM LUNAR OCCULTATIONS

Richard Allen Berg

St. Louis, Missouri

B.S., University of Illinois, 1964

M.A., University of Virginia, 1966

A Dissertation Presented to  
the Graduate Faculty of the  
University of Virginia  
in Candidacy for the Degree of Doctor of Philosophy

Leander McCormick Observatory  
University of Virginia

December

1969

## ABSTRACT

In search of angular structure in stellar sources, the Virginia dual-channel photometer was used at McCormick Observatory's Fan Mountain Station (32-inch reflector) and Kitt Peak National Observatory (#2 36-inch reflector) to record occultations of stars by the moon. A 50-50 beam-splitting mirror distributes the light to two EMI 6256 S/A photomultipliers operated at 1100v DC. A focal plane diaphragm admits an area of sky of 100 square seconds of arc, and UBV- and Strömgren- type filters are used to isolate spectral regions. The photoelectrons are fed through preamplifiers and amplifiers to an integrated-circuit photon counter with a capacity of twelve binary bits in each channel and a 1.04 millisecond time resolution. The binary bits are read out sequentially and recorded on a stereo tape recorder as a 12.5 khz. amplitude modulated square wave. Photon counts vs. time are later recovered from the tape and represent the basic data. The occultation curves are restored to strip-intensity profiles as a function of position by Scheuer's deconvolution technique (1962, Australian J. Phys., 15, 333). The results of observations of seven occultations are summarized here. Upper limit values quoted below represent mean errors of observation.

BD -18°6037 (HD 208482, 6.6, A0) has an angular diameter  $< 0''.0016$  with no indication of duplicity. BD +23° 505 (HD 23288, 5.23, B7IV) is a newly discovered double star with separation  $0''.0062 \pm 0''.0002$  at scan position angle  $247^\circ$ ,  $\Delta m_B = 2.0 \pm 0.2$ . The diameter of the primary is  $< 0''.0016$ . The known spectroscopic binary BD +23° 507 (HD 23302, 3.59, B6III) has an observed diameter of  $0''.0030 \pm 0''.0018$  m.e., but this value is affected by the presence of the secondary component which is  $< 0''.0025$  distant at scan position angle  $108^\circ$ . The duplicity of BD +24° 547 (HD 23338, 4.19, B6V) is not confirmed. The separation in scan position angle  $22^\circ$  is  $< 0''.0015$ ; for this occultation the

observed lunar slope at the point of disappearance is  $4^{\circ}1 \pm 0^{\circ}1$ . BD +23° 540 (HD 23642, 6.61, AOV), a known spectroscopic binary, likewise is not seen as a double. The observed diameter is  $< 0''.0021$ . BD +23° 536 (HD 23629, 6.19, AOV) has an observed diameter of  $0''.0104 \pm 0''.0017$  m.e., fully fifty times larger than the computed blackbody diameter. Restorations do not disclose a secondary component but do show evidence of lunar limb irregularities. For BD +23° 541 (HD 23630, 2.77, B7III) the observed diameter is  $< 0''.0018$ , and no evidence for duplicity is seen.

In terms of gross angular structure, occultations of stars provide excellent opportunities for discovery of very close binaries, especially those with low inclination orbits where spectroscopic methods fail. Angular diameter determinations are sensitive to signal/noise, bandwidth smoothing, aperture smoothing, and time constant smoothing. Using the instrumental system described here, the practical limit to resolution is on the order of  $0''.001$  and is set principally by bandwidth smoothing.

## TABLE OF CONTENTS

I.	Historical Background . . . . .	1
II.	Theoretical Developments . . . . .	8
	A. Occultation Curves . . . . .	8
	B. Restorations . . . . .	11
	C. Diameter Determination . . . . .	15
	D. Limb Darkening . . . . .	16
III.	Instrumentation . . . . .	19
IV.	Observations and Results . . . . .	28
	A. BD -18°6037 (V) . . . . .	33
	B. BD -18°6037 (B) . . . . .	35
	C. BD +23° 505 (B) . . . . .	37
	D. BD +23° 507 (y) . . . . .	42
	E. BD +24° 547 (V) . . . . .	45
	F. BD +24° 547 (B) . . . . .	47
	G. BD +23° 540 (B) . . . . .	49
	H. BD +23° 536 (B) . . . . .	51
	I. BD +23° 541 (b) . . . . .	55
	J. BD +23° 541 (y) . . . . .	57
	K. Other Occultations . . . . .	59
V.	Remarks . . . . .	62
	A. Lunar Slopes . . . . .	62
	B. Angular Separation, Parallax, and Orbital Inclination . . . . .	66
	C. Photon Counter Capability . . . . .	69
	D. Restorations of Model Occultations . . . . .	71
VI.	Appendix: Model Occultation Curves . . . . .	76
VII.	References . . . . .	81
VIII.	Acknowledgments . . . . .	83

## LIST OF TABLES

Table 1.1. Operating Characteristics of Photoelectric Systems (Evans 1951) . . . . .	5
Table 3.1. Filter-photomultiplier Parameters . . . . .	21
Table 3.2. Theoretical Coincident Pulse Rates . . . . .	26
Table 4.1. Cross-identification List . . . . .	28
Table 4.2a. Occultation Prediction Data . . . . .	30
Table 4.2b. Occultation Observation Data . . . . .	30
Table 4.3. Observed Stellar Diameters . . . . .	31
Table 4.4. Restoration Data, BD -18°6037 (V) . . . . .	33
Table 4.5. Restoration Data, BD -18°6037 (B) . . . . .	35
Table 4.6. Restoration Data, BD +23° 505 (B) . . . . .	37
Table 4.7. Restoration Data, BD +23° 507 (y) . . . . .	42
Table 4.8. Restoration Data, BD +24° 547 (V) . . . . .	45
Table 4.9. Restoration Data, BD +24° 547 (B) . . . . .	47
Table 4.10. Restoration Data, BD +23° 540 (B) . . . . .	49
Table 4.11a. Restoration Data, BD +23° 536 (B) . . . . .	51
Table 4.11b. Restoration Data with Corrected Limb Velocity, BD +23° 536 (B) . . . . .	52
Table 4.12. Restoration Data, BD +23° 541 (b) . . . . .	55
Table 4.13. Restoration Data, BD +23° 541 (y) . . . . .	57
Table 4.14. Occultations of Stars That Could Not Be Recovered From the Data Tape . . . . .	60
Table 4.15. Occultations of Stars That Were Recovered But Not Analyzed . . . . .	61
Table 5.1. Axis Angles and Elevations at LIBA 2.10, LIBB -5.67 . .	65
Table 5.2. Orbital Data of Spectroscopic Binaries . . . . .	68
Table 5.3. Observations of Standard Stars at Kitt Peak . . . . .	69
Table 5.4. Recovered Diameters of Test Sources . . . . .	72

## LIST OF FIGURES

Figure 1.1.	Michelson's Stellar Interferometer . . . . .	3
Figure 1.2.	A Simplified Diagram of an Intensity Interferometer .	6
Figure 2.1.	$I(w)$ vs. $w$ . . . . .	9
Figure 3.1.	Relative Response of the Photometer . . . . .	20
Figure 3.2.	Example of One Data Record . . . . .	22
Figure 3.3.	Pulse Counting Photometer Logic . . . . .	23
Figure 3.4.	Dual-channel Photometer . . . . .	25
Figure 3.5.	The Photon Counter and Accessories . . . . .	25
Figure 4.1.	Photon Count vs. Time, BD $-18^{\circ}6037$ (V) . . . . .	34
Figure 4.2.	Photon Count vs. Time, BD $-18^{\circ}6037$ (B) . . . . .	36
Figure 4.3.	Photon Count vs. Time, BD $+23^{\circ} 505$ (B) . . . . .	39
Figure 4.4.	Restoration Curves for BD $+23^{\circ} 505$ . . . . .	40
Figure 4.4a.	Radial Velocities vs. Phase ( $P = 90$ days) . . . . .	41
Figure 4.5.	Photon Count vs. Time, BD $+23^{\circ} 507$ (y) . . . . .	43
Figure 4.6.	Restoration Curves for BD $+23^{\circ} 507$ . . . . .	44
Figure 4.7.	Photon Count vs. Time, BD $+24^{\circ} 547$ (V) . . . . .	46
Figure 4.8.	Photon Count vs. Time, BD $+24^{\circ} 547$ (B) . . . . .	48
Figure 4.9.	Photon Count vs. Time, BD $+23^{\circ} 540$ (B) . . . . .	50
Figure 4.10.	Photon Count vs. Time, BD $+23^{\circ} 536$ (B) . . . . .	53
Figure 4.11.	Restoration Curves for BD $+23^{\circ} 536$ . . . . .	54
Figure 4.12.	Photon Count vs. Time, BD $+23^{\circ} 541$ (b) . . . . .	56
Figure 4.13.	Photon Count vs. Time, BD $+23^{\circ} 541$ (y) . . . . .	58
Figure 5.1.	Occultation Geometry . . . . .	64
Figure 5.2.	Lunar Profile for the Occultation of BD $+24^{\circ} 547$ . . .	65
Figure 5.3.	Lunar Slopes, $\xi$ , $\xi = \xi(R, \zeta)$ . . . . .	67
Figure 5.4.	Counts vs. One-sigma Dispersion . . . . .	70
Figure 5.5.	$f(x) = g(x)*t(x)$ . . . . .	74
Figure A.1.	Model Occultation Curves . . . . .	79
Figure A.2.	Model Occultation Curves . . . . .	80



## I. Historical Background

Stellar diameters represent data of fundamental theoretical importance in astronomy. The stellar radius is a parameter in the study of stellar evolution and stellar interiors, of the mass-radius relation, and of eclipsing binary systems.

The stellar diameter can be computed approximately from radiation laws using the relation

$$L = 4\pi R^2 \sigma T_e^4 \quad (1.1)$$

where  $L$  and  $T_e$  are determined observationally. A value determined in this way can be in error because stars do not radiate as black bodies. By measuring stellar diameters directly and independently of the radiation laws, empirical corrections to the effective temperature scale can be found.

Gray (1967) describes a method by which stellar radii can be determined by measuring  $F_\nu$ , the monochromatic flux received at the earth. By comparing  $F_\nu$ , observed at several wavelengths, to the energy distribution predicted from model atmosphere computation (which is a function of  $T_e$ ), the radius of the star can be found by

$$R = r \sqrt{F_\nu / f_\nu}, \quad (1.2)$$

with  $r$  = the distance to the star (an observed quantity), and  $f_\nu$  = the monochromatic flux at the star's surface (a computed quantity). If, instead, one independently measures the angular diameter of a star, the problem is inverted and the absolute monochromatic flux at the star's surface can be determined from

$$f_\nu = \frac{4F}{\theta^2} \quad (1.3)$$

with  $\theta = 2R/r =$  the angular diameter. Again the effective temperature can, in principle, be determined since

$$\int_0^{\infty} f_{\nu} d\nu = \sigma T_e^4 \quad (1.4)$$

The stellar diameter can be computed for those eclipsing systems where both photometric and spectroscopic observations are available. The photometric information gives the orbital inclination,  $i$ , the radius of each star in terms of the semi-major axis, and the luminosity of each star in terms of the total luminosity of the system. Radial velocity information provides the semi-major axis,  $a \sin i$ . Thus the radius of each star is determined. But if one independently determines the angular diameters of the stars from occultations, one can use the photometric and spectroscopic data to derive a parallax for the system and the absolute luminosity of each star.

The independent, geometric determination of stellar diameters is an imposing task because of the small angles which must be measured. In the early years of this century, Michelson (1920) described an experiment to measure the fringe visibility and position produced by the interference of two separate beams of light from a single star. Mounted on the front end of the 100-inch Hooker telescope, the equipment consisted of a single rigid bar on which two fixed mirrors,  $M_f$ , and two movable mirrors,  $M_m$ , were attached. Figure 1.1 shows the instrument schematically. Michelson and Pease (1921) showed that the small angular diameter of a star would produce interference fringes at the focus of the instrument when the movable mirrors were close together, but the fringes would disappear at wider spacings. Further, they showed that the fringe visibility was a function of the angular diameter of the star. The first zero of the fringe visibility curve is related to the spacing of the movable mirrors,  $b$ , and the angular diameter,  $\phi$ , by the simple equation  $b = 1.22\lambda/\phi$ , where  $\lambda$  is the wavelength of observation.

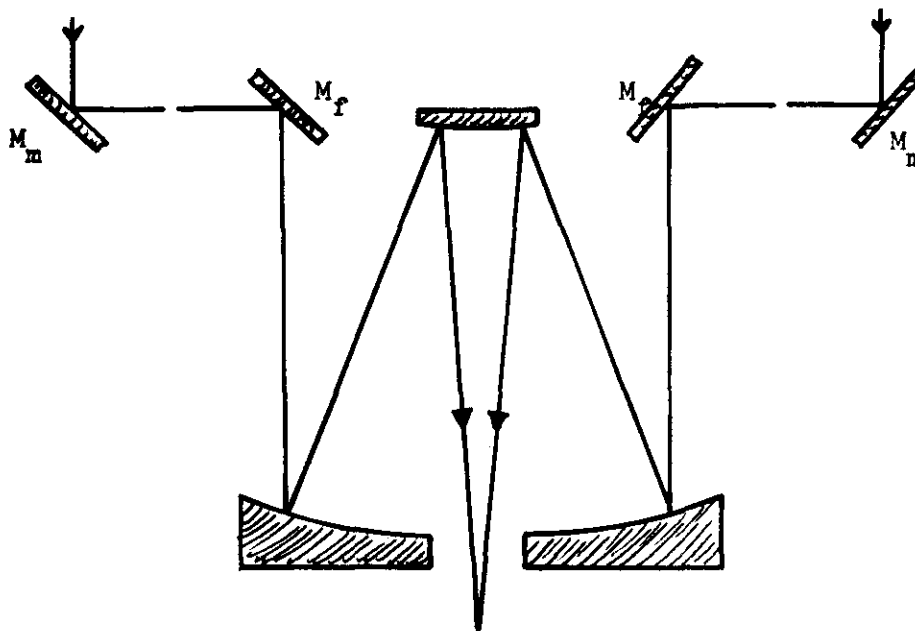


Fig. 1.1.--Michelson's Stellar Interferometer

The earliest observations were made with mirrors whose maximum separation was twenty feet, giving a lower limit to resolution of about 0.02 seconds of arc at 5000Å. A slightly lower limit could be reached by extrapolation from measurements of fringe visibility at shorter mirror spacings. Angular diameters for seven stars were obtained with this instrument. The stars are all K or M giants or supergiants, since they were the ideal and only objects within the capability of their instrument. A second instrument, with a maximum mirror spacing of fifty feet, was built about ten years later (Pease 1930). The diameters of an additional four stars were found. Three stars on the first observing list were reobserved, and for only one of them-- $\alpha$  Sco--was the original value of the diameter not reconfirmed. No estimates on accuracies for these diameters are given by Michelson or Pease, but Brown (1968b) estimates that "the standard error

increased with baselength and probably lay in the range 10 to 20 percent." Because the structural rigidity of the instrument was critical to the accuracy of the results, the list of stars which the interferometer was able to measure (angular diameters  $> 0''.008$ ) was quickly exhausted.

As early as 1908 it had been suggested that lunar occultations might offer the possibility of determining stellar diameters. McMahon (1908) had proposed timing the disappearance of stars behind the lunar limb and from the known speed of the limb getting the diameter in a strictly geometric sense. Eddington (1909) pointed to the diffraction effect at the limb which would spoil that measurement--a point source would have a spurious diameter of 0.008 seconds of arc. Thirty years later Williams (1939) showed how the diffraction effect itself could be used to derive stellar diameters. Whitford (1939) made observations of  $\beta$  Cap and  $\nu$  Aqr on September 6-7, 1938, using a fast-response photoelectric system on the 100-inch Hooker telescope, an oscilloscope, and a moving film camera. Although Whitford's data did not reveal values for the diameters his observations represent the first photoelectric high resolution recordings of occultations of stars by the moon.

In the period 1950-1952 a number of occultations of Antares were observed by several investigators. Cousins and Guelke (1953) used an RCA 931A photomultiplier attached to the 24-inch Victoria (Cape Observatory) refractor, recording an oscilloscope deflection with a moving film camera, for the occultations of 4 May 1950, 15 July 1951, 13 April 1952, and 8 March 1953. Using a galvanometer recording on bromide paper, Evans, Heydenrych, and van Wyk (1953) observed the 13 April 1952 occultation with the 74-inch Radcliffe (Pretoria) reflector and an EMI photomultiplier. For the 8 March 1953 occultation Evans (1955) used an RCA 931A photomultiplier with the galvanometer-bromide recorder at the 16-inch Rockefeller (Union Observatory) refractor. The occultation of 27 June 1950 was observed by Evans (1951) at

Pretoria with an RCA 931A photomultiplier. The operating characteristics of Evans' equipment, Table 1.1, are described in detail in his papers and are probably typical of the state-of-the-art of that period. Although analysis

TABLE 1.1

Operating Characteristics of Photoelectric  
Systems (Evans 1951)

Anode dark current	1/4 $\mu$ amp
Average sensitivity	10 amp/Lumen
Current amplification	$10^6$
Circuit time constants	1.65 msec.
Galvanometer undamped frequency	580 hertz
Recording paper speed	10 ips.

of each occultation was carried out by the individual investigators, Evans (1957) made a comparative study of all Antares occultations, some of which had been observed from two locations. A mean observed diameter of  $0''.041 \pm 0''.001$  (pe) was determined. Evans concludes that gross limb irregularities do not exist in general for any occultation, but a correction of -3% should be applied to account for the gentle, sloping irregularities, yielding a diameter of  $0''.040 \pm 0''.001$  (pe) for Antares. Evans cautions that a circular disc, whatever the symmetric law of darkening assumed, does not reproduce the observed occultation curve for Antares. The difference occurs at the "toe" of the curve (near zero intensity) where the observed intensity is 5% higher than the computed intensity.

A recent paper by Taylor (1966) reexamines these Antares occultations using Scheuer's convolution process to determine the radial brightness distribution across the stellar disc (Scheuer 1962; see also Chapter 2). Antares, Taylor finds, is composed of a core-component with approximately uniform brightness and of  $0''.019 \pm 0''.003$  radius containing  $80\% \pm 10\%$  of the flux, and a halo- or shell-component extending to  $0''.028 \pm 0''.004$  radius, accounting for the remaining flux.

An unusual instrumental approach was developed by Brown and Twiss for measuring angular stellar diameters. The intensity interferometer (Brown, Davis and Allen 1967) operates like the Michelson stellar interferometer except that no attempt is made to preserve the phase of the incident light. The signals from two photocells are multiplied after detection rather than added prior to detection, as in Michelson's interferometer. Figure 1.2 is a schematic illustration of the intensity interferometer (Brown 1968b). In the intensity interferometer light from a single star is focussed by two separate reflectors onto two photomultipliers. The output currents are amplified and then correlated in a linear mixer. The correlation is proportional to the square of the fringe visibility which would be observed with the same spacing by a classical Michelson interferometer. Thus, it is possible to measure this correlation at various spacings and find the angular diameter.

Two advantages of the intensity interferometer are its very high resolution ( $0''.0005$ ) and its insensitivity to atmospheric scintillation. The cost for this performance is that one is limited to observing stars brighter than apparent magnitude +2 and earlier than spectral class F5. In

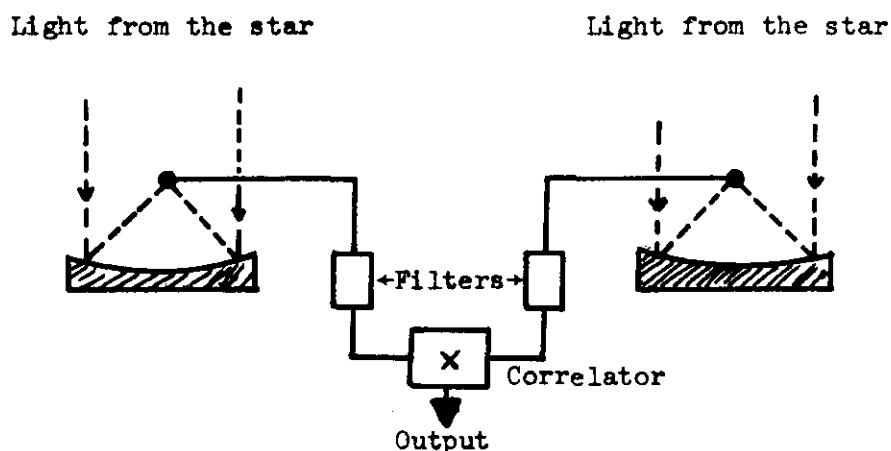


Fig. 1.2.--A Simplified Diagram of an Intensity Interferometer (Brown 1968b)

addition, very long integration times are needed to achieve satisfactorily low probable errors, an example being 40 hours for 5% precision for a star with an apparent blue magnitude of +1. Fifteen angular diameters have been measured to accuracies better than 10% in a few years of operation (Brown 1968a).

Recently a number of investigators have renewed interests in occultations and have begun observational programs on a continuing basis. Rakos (1967) used the 42-inch Lowell reflector with an EMI 6256 S/A photomultiplier, an oscilloscope, and a moving film camera to observe seventeen stellar occultations. He computed the diameters of two of them, 80 Vir ( $m_v = 5.75$  KO,  $\phi = 0''.0022 \pm 0''.0001$ ) and  $\nu$  Vir ( $m_v = 4.20$  MO,  $\phi = 0''.00565 \pm 0''.00001$ ), and he disclosed the binary nature of a third, HD 75974. The remainder have "exceedingly small apparent diameters." Rakos estimates the attainable errors at a few percent for the brighter stars to about 10% for fainter stars. Nather (1969) is using a 400-channel analyzer as a pulse counter and hopes to equip a telescope with a four-channel photometer. Herr (1969) has published a list of spectroscopic and eclipsing binaries which can be occulted by the moon.

The observations in the present investigation were undertaken with three purposes: 1) to minimize "analog" interpretive processes in the data acquisition by building and using a special pulse-counting photometer unit, amplifiers, and logic circuitry, 2) to apply Scheuer's (1962) restoration process at optical wavelengths, and 3) to look for angular structure in stellar sources. The analytical representation of occultation curves, the restoring process, limb darkening, and other theoretical considerations are discussed in Chapter 2. Chapter 3 is a discussion of the instrumental system and its parameters, and Chapter 4 is a tabulation of observations and analysis of the data. A discussion of errors and additional information comprise the last chapter.

## II. Theoretical Developments

### A. Occultation Curves.

The development of theoretical occultation curves follows directly from the theory of Fresnel diffraction at a straight edge. At optical wavelengths occultation events occur at a scale of only a few meters on the lunar limb. Thus the straight-edge assumption is valid for these observations. For a plane, monochromatic wave diffracted by a straight edge the intensity is given (Born and Wolf 1964) by

$$I(w) = \frac{I_0}{2} \left[ \left( \frac{1}{2} + C_w \right)^2 + \left( \frac{1}{2} + S_w \right)^2 \right]. \quad (2.1)$$

Here  $I_0$  is the freespace intensity,  $C_w$  and  $S_w$  are the Fresnel integrals

$$C_w = \int_0^w \cos \frac{\pi u^2}{2} du \quad \text{and} \quad S_w = \int_0^w \sin \frac{\pi u^2}{2} du, \quad (2.2)$$

and  $w$  is a unitless parameter defined by

$$w = h_0 \sqrt{\frac{2(a+b)}{\lambda ab}} \quad (2.3)$$

with  $h_0$  = the perpendicular distance, diffracting edge to source center,

$a$  = distance of source behind the diffracting edge,

$b$  = distance of the observer in front of the edge, and

$\lambda$  = the wavelength of observation.

For stellar phenomenon  $a \gg b$ , and equation (2.3) reduces to

$$w = h_0 \sqrt{\frac{2}{\lambda b}} \quad (2.4)$$

If  $v_r$  is the speed of the lunar limb (in seconds of arc per second) in the direction normal to the limb with  $v_r < 0$  for disappearances, and  $t$  is the time (in seconds) measured from geometric occultation with  $t < 0$  preceding occultation, then the physical circumstances of each occultation,  $v_r$ ,  $t$ ,  $b$ ,



and  $\lambda$  can be related to the curve  $I(w)$  by

$$w = 4.8481 \times 10^{-6} v_r t \sqrt{\frac{2b}{\lambda}} \quad (2.5)$$

The function  $I(w)$  is an unique curve defined solely by the Fresnel integrals. Figure 2.1 is a graph of  $I(w)$  vs.  $w$ . At geometric occultation  $w = 0$  and the intensity is  $0.25 I_0$ ; the first maximum occurs at  $w = 1.225$ ,

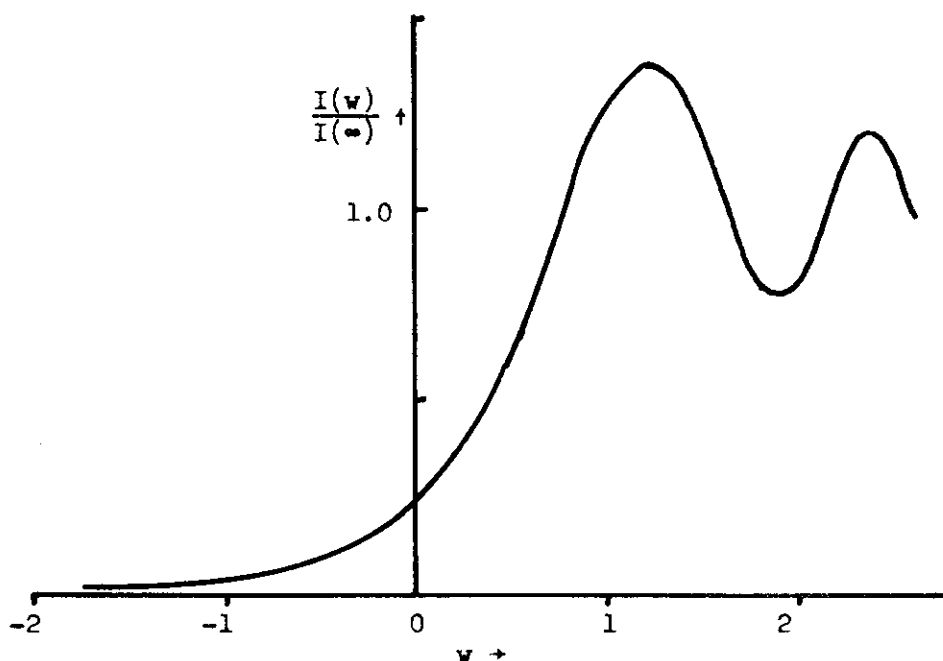


Fig. 2.1.-- $I(w)$  vs.  $w$

where  $I = 1.37 I_0$ ; the second maximum occurs at  $w = 2.345$  with the intensity equal to  $1.20 I_0$ .

When considering a star that is not a point source, one must divide the star into "pointsource" elemental areas and perform an integration over the surface. The process amounts to convolving the true brightness distribution with the diffraction pattern. Equation (2.1) is used for each element and is normalized to an appropriate value to account for wavelength, limb darkening, and projection effects. The total intensity due to an extended source in the influence of Fresnel diffraction is given by the following power series

$$I_{\lambda}(h_0) = I_{\lambda}(h_0) + \sum_{n=0}^{\infty} d^{2n} I_{\lambda}(h_0) \frac{\rho^{2n}}{(2n)!} \left( \frac{(1-\beta_{\lambda}) + \frac{2^{n+2}}{(2n+1)(2n+3)} \beta_{\lambda}}{1 - 1/3 \beta_{\lambda}} \right) \quad (2.6)$$

where  $\beta_{\lambda}$  is the limb darkening coefficient,  $0 \leq \beta_{\lambda} \leq 1$ , and  $\rho$  is the reduced radius,  $\rho = b\phi/2$ , with  $\phi$  as the angular diameter. The derivation of equation (2.6), based on a similar derivation by Diercks and Hunger (1952), is the subject of the Appendix.

The series solution is a quick computer algorithm. However, the derivatives of  $I_{\lambda}(h_0)$  do not tend toward zero for large  $h_0$ , and, in combination with increasing powers of  $\rho$ , cause the series to diverge for large  $\rho$ . To produce theoretical curves for larger diameters one must resort to numerical integration. A solution can be found using fourth-order Runge-Kutta integration. Equation (A.5) is rewritten in its integral form as

$$I_{\lambda}(h_0) = \sum_{i=-1}^1 A_{\lambda}(x_i) \left( \left( \int_0^{\kappa} \cos \frac{\pi u^2}{2} du + 1/2 \right)^2 + \left( \int_0^{\kappa} \sin \frac{\pi u^2}{2} du + 1/2 \right)^2 \right) \Delta x_i, \quad (2.7)$$

where  $\kappa = h_0 + x\rho$ . The computation of the integral then involves evaluation of the integrand at various points and summation. Although slow by comparison with the series expansion, the results can be made quite accurate by adjusting the integration step size,  $\Delta x_i/2$ .

Using equation (2.7), occultation curves have been generated in both graphical and punch-card formats for diameters from 0".000 to 0".010. The graphs, appearing in the Appendix, serve to illustrate how the diameter qualitatively affects the appearance of the occultation. The punch-card format is useful as quantitative input for checking the procedures used to analyze the data.

Not considered in this development are the effects of lunar limb roughness, stellar brightness anomalies such as large prominence activity, polychromaticity (bandwidth smoothing), and telescope aperture smoothing.

It is important to remain aware of these influences; but when narrow interference filters (e.g. Strömgren type) and small apertures are used, only lunar limb roughness and stellar anomalies will seriously distort occultation curves. Stellar brightness anomalies can probably be approximated by assuming they are "equivalent double" sources of appropriate dimensions. Lunar limb roughness of the order of meters in magnitude is a more severe problem. Details of this effect have been discussed by Diercks and Hunger (op. cit.), but as observations seem to indicate (Rakos 1964, Evans 1957), the probability of encountering severe limb features is low.

#### B. Restorations.

The restoration of occultation curves occurs in two steps. First, the strip-integrated brightness distribution and diameter are found. Only then can the transformation to a radial brightness distribution and limb darkening be made, assuming that the star is radially symmetric. Only for stars having extreme photospheric activity is the assumption not valid.

The restoration process used to recover strip-integrated brightness distributions in these analyses is described in detail by Scheuer (1962) and again by von Hoerner (1964). Defining  $f(x)$  as the observed diffraction pattern,  $p(x)$  as the Fresnel diffraction pattern, and  $t(x)$  as the true (strip-integrated) brightness distribution, then the observed diffraction curve is the true brightness distribution convolved with the Fresnel diffraction curve, or

$$f(x) = p(x) * t(x) \quad (2.8)$$

where "\*" is the convolution operation. Equation (2.8) is analagous to equation (A.5). By the convolution theorem

$$F(v) = P(v)T(v) \quad (2.9)$$

where  $P(v)$  is the Fourier Transform of  $p(x)$ , etc. If  $P(v) \neq 0$  for all  $v$ ,

$$T(v) = \frac{F(v)}{P(v)}. \quad (2.10)$$

Applying the convolution theorem,

$$\begin{aligned} t(x) &= \text{function whose Fourier Transform is } 1/P(v)*f(x) \\ &= \text{Fourier Transform of } 1/P(-v)*f(x) \end{aligned} \quad (2.11)$$

or

$$t(x) = c(x)*f(x) \quad (2.12)$$

Thus the true brightness distribution can be recovered from the observed occultation curve by convolution with a suitable function. The existence of  $P(v)$  is not questioned here; the restoring function was shown by Scheuer to be

$$c(x) = a^2 p''(-x)$$

where  $a = 1/\lambda b$ , and  $p''(x)$  is the second derivative of  $p(x)$ . The amplitude of  $p''(x)$  increases linearly for large  $x$ , and since  $f(x)$  does not go to zero at large  $x$ , the convolution, equation (2.12), is not convergent. One must be content to restore the occultation curves to a strip distribution as if they had been scanned by a beam of finite width. Scheuer suggests using a gaussian beam,  $b(x) = \exp(-x^2/b^2)$ , so that

$$b(x)*t(x) = c'(x)*f(x) \quad (2.13)$$

with

$$c'(x) = b(x)*c(x) = a^2 e^{-x^2/b^2} * p''(x).$$

Increasingly smaller values of  $b$  for the gaussian beamwidth correspond to restorations of increasing resolution, for  $b(x) \rightarrow \delta$  as  $b \rightarrow 0$ , and  $\delta*t(x)=t(x)$ .

Equation (2.13) also indicates that the observed, restored brightness distribution curve is the convolution of a gaussian with the true strip brightness distribution.

von Hoerner (1964) applied Scheuer's process extensively to calculate a set of restoring functions,  $c'(x)$ , for various restoring beamwidths. He also investigated the restoring accuracy as a function of noise and bandwidth by restoring many model occultations. He determined the lower limit for the restoring beamwidth due to noise fluctuations to be

$$R_N > \frac{52''}{q_0^2} \quad (2.14)$$

where  $q_0$  is the observed signal/noise integrated over one arcsecond of the moon's motion (about 2.2 seconds). It is more convenient to express  $R_N$  in terms of the moon's motion over the actual integration time,  $\tau = 1.04$  milliseconds, for then the observed signal/noise ratio can be used. If  $v_r$  is the velocity of the moon in the direction normal to the surface of the limb, equation (2.14) is normalized by the factor  $v_r \tau$  to become

$$R_N > \frac{52'' v_r \tau}{q_0^2} . \quad (2.15)$$

If an average value of  $v_r$  is 0.35 seconds of arc per second, then the limiting restoration beamwidth is approximately  $R_N > 0.0189/q_0^2$ .

von Hoerner's lower limit for the restoring beamwidth due to wavelength smoothing of the diffraction pattern in a broad bandpass is

$$R_L > .616\sqrt{B\lambda} \quad (2.16)$$

where  $B$  is the bandwidth in percent of frequency,  $B = 100\Delta\nu/\nu$ ,  $\lambda$  is in meters, and the constant is for a gaussian passband. Changing  $B$  to wavelength units equation (2.16) is written

$$R_L > 0.616 \times 10^{-4} \sqrt{\Delta\lambda \{1 + \{\frac{\Delta\lambda}{2\lambda}\}^2 + \{\frac{\Delta\lambda}{2\lambda}\}^4 + \dots\}} \quad (2.17)$$

where  $\Delta\lambda$  is the bandwidth in angstroms and  $R_L$  is the limit in seconds of arc. The first order approximation suffices for most cases. If  $\Delta\lambda = \lambda$ , an error in  $R_L$  of 15% is made by ignoring the higher-ordered terms.

A limitation arises from the aperture smoothing of the diffraction curve at the telescope. Essentially one cannot resolve into elements those features which at the distance of the moon have a size less than the aperture of the telescope. Therefore  $R_A > a/b$ , where  $a$  is the telescope aperture and  $b$  is the distance to the moon. Expressing the aperture in inches and using a mean distance to the moon of  $3.848 \times 10^8$  meters,  $R_A$ , in seconds of arc, becomes

$$R_A > 13a \times 10^{-6}. \quad (2.18)$$

Taylor (1966) gives a value of  $R_A > 9a \times 10^{-6}$ . The aperture limit does not preclude using a rectangular mask of width "a" over the objective of diameter "d" ( $d > a$ ) when the mask is oriented parallel to the lunar limb.

The time constant used for observation also sets a limit. Obviously the angular resolution can never be better than that angle through which the moon moves in unit time constant. In seconds of arc this limitation is

$$R_T > v_r \tau. \quad (2.19)$$

One might expect the limitation set by noise fluctuations to determine the maximum restoring resolution. For a star of visual magnitude  $V$ , corresponding to the monochromatic flux at  $\lambda 5465$ , atmospheric extinction of  $A$  magnitudes, a telescope of aperture  $D$  inches, an integration time of  $T$  seconds, a bandwidth of  $L$  angstroms, and a quantum efficiency  $E$  (mirrors, filters, and photomultipliers), the signal/noise,  $Q$ , is found (Code and

Liller 1962) by

$$5\log Q = 9.24 + 5\log D + 2.5\log LT + 2.5\log E - V - A. \quad (2.20)$$

If  $L = 1000A$ ,  $E = .0288$ ,  $T = .00104$  seconds, and  $D = 32$  inches are typical values for broadband observations, equation (2.20) becomes

$$5 \log Q = 12.955 - V - A. \quad (2.21)$$

For a star of  $V = 5.555$ , with  $A = +.4$ , the predicted signal/noise is 25.

From equations (2.15-19)

$$R_N > 0".00003$$

$$R_L > 0".00195$$

$$R_A > 0".00042$$

$$R_T > 0".00036,$$

indicating that in this example noise fluctuations are the least important.

However, additional noise components are added by atmospheric scintillation, scattered moonlight on the sky, and direct observation of the lunar limb.

These causes conspire often to reduce the signal/noise by a large factor.

Thus for  $Q = 6$ ,  $R_N > 0".00053$ . Further, observations using narrower filters reduce the value of  $R_L$  while simultaneously reducing the signal/noise.

Observations of fainter stars also reduce  $Q$ . In general the highest restoring resolution is limited by both noise fluctuations and bandwidth smoothing.

### C. Diameter Determination.

There is little difficulty in determining the angular diameter for sources that are well resolved. When the sources are comparable to or smaller than the restoring beamwidths difficulty is encountered. For small sources upper limits to diameters are important parameters. When restoring the same occultation curve with functions of differing resolution, the noise components

of the occultation curve are weighted differently for those various restorations. A scheme for finding the weighted mean diameter and its error has been developed by von Hoerner (1965), is presented here, and is used in this investigation.

If  $b_1$  is the half-power width of the source on the restored curve and  $\Delta b_1$  is the estimated error of measuring  $b_1$ , then  $a_1 = b_1^2 - \Delta b_1^2 - b_r^2$  and  $\Delta a_1 = 2b_1 \Delta b_1$ , where  $b_r$  is the restoring beamwidth.  $\Delta b_1$  is estimated from the signal/noise of the observation by  $\Delta b_1 = k_b b_1 \sqrt{v_r \tau / q_0} \sqrt{b_r}$ , where  $k_b = 2.0 \pm 0.2$  (von Hoerner 1964). The weight of each measurement is  $w_1 = 1/\Delta a_1^2$ . If  $W = \sum w_1$ , then  $A = \frac{1}{W} \sum w_1 a_1$  and  $\Delta A = \frac{1}{W} \sum w_1 \Delta a_1$ . Finally, with  $x = A/\Delta A$ , the diameter and mean error are found from

$$\phi = \sqrt{A} \pm (1 + 1/x^2) \frac{\Delta A}{2\sqrt{A}} \quad x \geq 1 \quad (2.22)$$

$$\phi < \sqrt{|A| + \Delta A} \quad x < 1 \quad (2.23)$$

Equation (2.22) gives the weighted mean value of the diameter and the mean error when the mean error of computing  $A$ ,  $\Delta A$ , is smaller than  $A$ . In other cases only an upper limit for the diameter is computed with equation (2.23).

#### D. Limb Darkening and Radial Brightness Distribution.

A limb darkening effect is of importance because it provides direct observational evidence that a temperature gradient exists in stellar atmospheres. The equation for limb darkening can be derived from the equation of radiative transfer. In its most general form it is written

$$I_v(0, \theta) = S_v(\tau_v) e^{-\tau_v \sec \theta} \sec \theta \, d\tau_v \quad (2.24)$$

where  $S_v(\tau_v)$  is the source function and  $\tau_v$  is the optical depth. If the stellar material is in thermal equilibrium  $S_v(\tau_v)$  can be replaced with the Planck function. Then the wavelength dependence is such that limb darkening increases with decreasing wavelength. By making use of Eddington's approxi-



mation it can be shown (Aller 1963) that the limb darkening, as a function of emergence angle,  $\theta$ , for a grey body in integrated light, is

$$\frac{I(\theta)}{I(0)} = 1 - \frac{3}{5} + \frac{3}{5}\cos\theta. \quad (2.25)$$

Defining a limb darkening function  $\phi_\lambda(\mu)$  as

$$\phi_\lambda(\mu) = \frac{I_\lambda(\theta)}{I_\lambda(0)} \quad \text{and} \quad \mu = \cos\theta \quad (2.26)$$

$\phi_\lambda(\mu)$  can be written as

$$\phi_\lambda(\mu) = A_\lambda + B_\lambda\mu \quad (2.27a)$$

or better (Aller 1963)

$$\phi_\lambda(\mu) = A_\lambda + B_\lambda\mu + C_\lambda(1 - \mu\ln(1+\mu^{-1})) \quad (2.27b)$$

for radiative equilibrium, and for convective equilibrium

$$\phi_\lambda(\mu) = \mu^k. \quad (2.28)$$

Limb darkening data of good quality,  $\phi_\lambda(\mu)$  vs.  $\mu$ , can be used to determine the general type of energy transport in stellar atmospheres by comparison with equations (2.27) or (2.28). If observations of  $\phi_\lambda(\mu)$  are made at various wavelengths, the temperature distribution  $T(\tau_\lambda)$  and some information regarding the wavelength variation of the continuous absorption coefficient can also be found for radiative atmospheres.

A single occultation observation, except for the very brightest stars, will not provide good limb darkening data. Taylor (1966) averaged five occultations of Antares ( $V = 0.89$ ) to derive radial brightness and limb darkening. He transformed the strip-integrated brightness distribution to radial brightness distribution assuming radial symmetry by an inverse Abel transformation (Bracewell 1956), compared  $\phi_\lambda(\mu)$  vs.  $\mu$  with equations of the form above, and concluded that the observed distribution fit neither

approximation very well.

Assume that the signal/noise of a sum of observations of equal signal/noise is proportional to the square root of the number of observations. To equal the signal/noise of Taylor's averaged "observations" would require about 215 observations of a  $V = 5.0$  star and 34 observations of a  $V = 3.0$  star. An approximate relation is

$$\log N = .4\{V + .835\}. \quad (2.29)$$

If current observing techniques have improved to the extent that one observation of Antares today would be as good as the five Taylor averaged, the situation is somewhat improved. Only 44 observations of a  $V = 5.0$  star, or seven observations of a  $V = 3.0$  star, would be required.

At the beginning of a program of occultation observations one is bound usually to have just a single observation per star. It requires many years of coordinated efforts to provide sufficient data for the accurate determination of limb darkening or radial brightness distribution. In the meantime one must be content to derive only the angular diameters.

### III. Instrumentation

A dual-channel photometer (Wood and Lockwood 1967) was mounted at the cassegrain focus and was used for all observations, although in many cases it was used in the single-channel mode. The photometer utilizes a 50/50 beam-splitting mirror, two six-cell filter wheels, and two temperature regulated thermoelectric cooling chambers for the EMI 6256 S/A photomultipliers. The photomultipliers, chosen for their low dark currents, have an S"Q" sensitivity curve. When operated at 1750 volts overall, the manufacturer rates the anode sensitivity at 2000 amperes/Lumen, the current gain at  $40 \times 10^6$  and the anode dark current at  $5 \times 10^{-4}$   $\mu$ amperes.

Six filters are used in the dual-channel photometer. They are similar to the Johnson B and V filters and the Strömberg u,v,b,y filters and have been identified B,V,u,v,b, and y. Transmission curves for these filters appear elsewhere (Doremus 1968, Berg 1967). The relative response of the photometer--the product of the % filter transmission and the % quantum efficiency of the photomultiplier--is given in Figure 3.1. The effective wavelengths of each bandpass have been computed from

$$\lambda_{\text{eff}} = \frac{\int \lambda T(\lambda) d\lambda}{\int T(\lambda) d\lambda} = \frac{\sum \lambda_i T_i(\lambda) \Delta \lambda}{\sum T_i(\lambda) \Delta \lambda} \quad (3.1)$$

where  $T(\lambda)$  is the relative response of the photometer. The bandwidth at the half-response point,  $\Delta \lambda$ , is approximated from the figure. The rectangular 100% width of each filter--that is, the width of a 100%-responding rectangular filter passing an equivalent amount of energy--is found by graphical approximation. The data for the filter-photomultiplier parameters are given in Table 3.1.

Although previous investigators have had success in recording and measuring occultation curves on moving film or sensitive paper, these

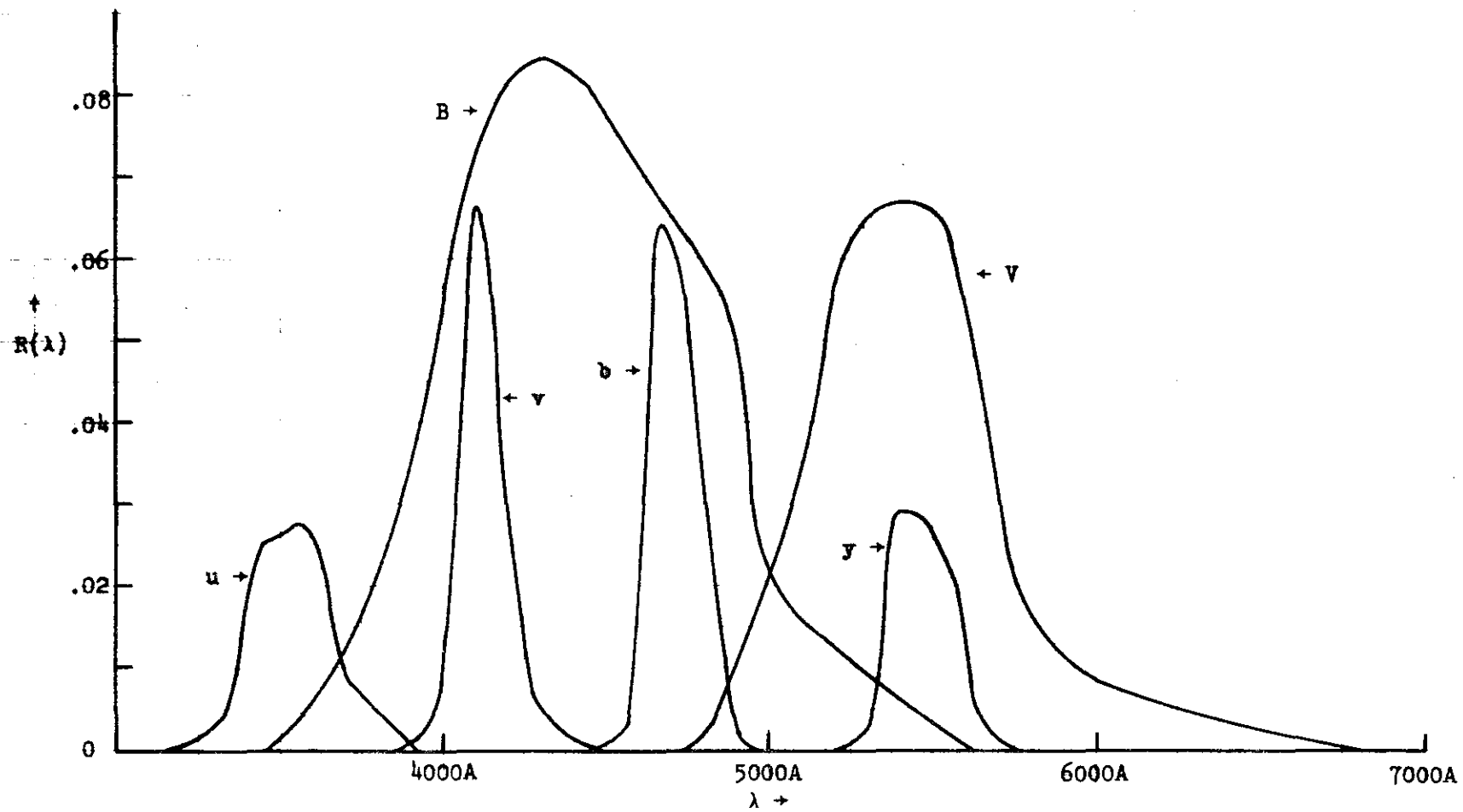


Fig. 3.1.--Relative Response of the Photometer

TABLE 3.1

Filter-photomultiplier Parameters			
Filter	$\lambda_{\text{eff}}(\text{\AA})$	$\Delta\lambda(\text{\AA})$	Rectangular 100% Width(A)
B	4440	994	83.6
V	5470	613	47.8
u	3530	297	8.6
v	4100	152	10.8
b	4680	187	12.1
y	5450	240	7.2

procedures are analog in nature. They can be complicated by nonlinearities in amplifiers, variable RC circuits and changing time constants, and personal error. To eliminate these problems, recording the occultations is accomplished with a pulse counting device specially designed and built for these observations. All systems are built in duplicate to allow simultaneous two-color observations to be made.

The counter consists of a preamplifier attached directly to the photomultiplier anode, an amplifier connected to the preamplifier through a 15 foot RG/58U cable, a digital twelve-bit binary counting circuit, a twelve-bit memory register, and necessary logic and switching circuitry. A crystal controlled oscillator fixes the minimum integration time at  $0.00104$  seconds. The integration time can be lengthened in factors of two up to  $2^{10} \times 0.00104$  seconds. The crystal is not temperature stabilized. The photoelectric pulses are continuously fed directly to the binary counter by way of the amplifiers. At intervals equal to the integration time a signal causes, in turn, the memory to be cleared, the counter bit configuration to be transferred to memory, and the counter to be cleared to zeroes. The total measured time during which these operations occur amounts to no more than  $1.5 \mu\text{seconds}$ . During the integration cycle the memory register, containing the binary count of the previous integration cycle, is read out serially

onto magnetic tape as a 12.5 kilohertz square wave modulated by the bit configuration. Figure 3.2 schematically shows a typical data "record" for a count of 189. The low-order binary digits are to the left, and a negative bit is provided as a flag indicating the beginning of the record. Data from each channel is recorded on a Sony, Model TC-200, stereo tape recorder.



Fig. 3.2.--Example of one data record.

The dual emitter-follower preamplifier accepts negative pulses from the photomultiplier, inverts the polarity, and presents positive low impedance pulses to the amplifier through a length of cable. The amplifier is a two-transistor circuit providing sufficient gain for the pulses to trigger the input counter gate. There is no discriminator in the circuit--the "discriminator level" is set by the threshold at which the input gate changes state (1.5 volts). Under operational conditions it is noted that the anode dark current from each photomultiplier produces somewhat less than one count during a 1.04 millisecond integration cycle. In addition, when observing a star against the dark sky, the resultant counts are independent of changes in the photomultipliers in the sense that small changes of a few tens of volts in the overall operating voltage do not change the number of pulses being counted. Power for the preamplifiers and amplifiers comes from internal 9-volt mercury cell batteries. Power for the counting and logic circuits is provided by a Lambda, Model LM252, regulated power supply. Figure 3.3

illustrates the interconnection of logical units of the pulse counter.

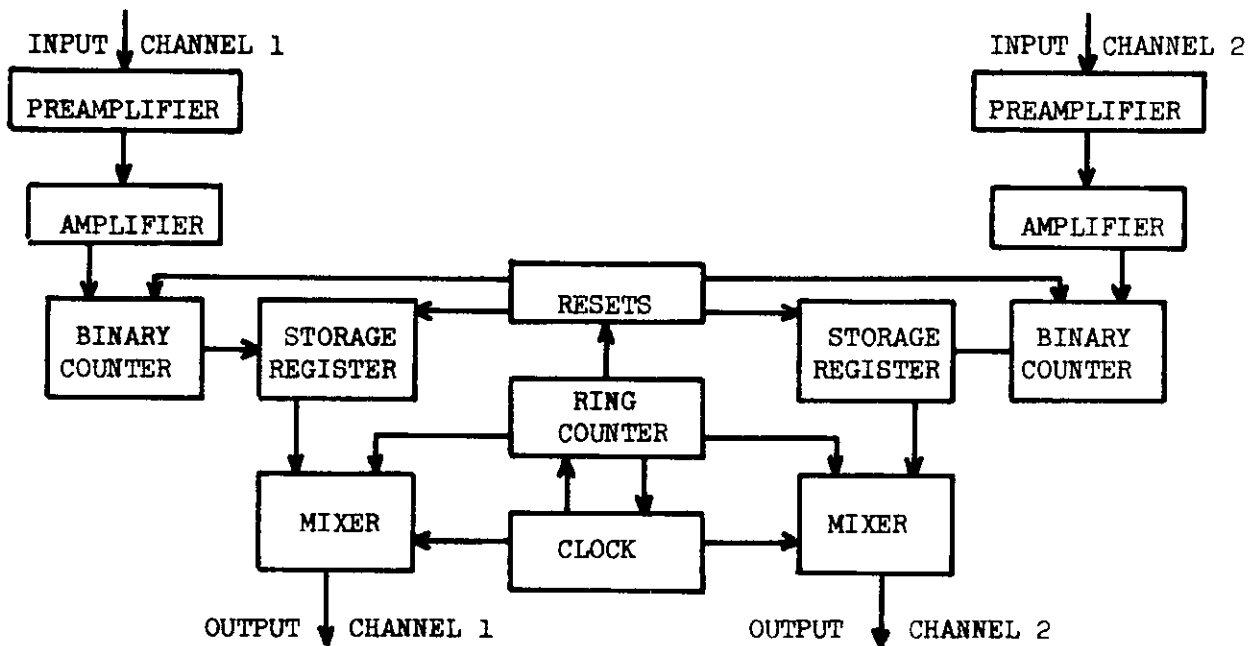


Fig. 3.3.--Pulse Counting Photometer Logic

Recovery of the digital data is accomplished in the following manner. The original data tape, recorded at 7 1/2 inches-per-second (12.5 khz.) is first played to an oscilloscope to determine the point on the tape at which the occultation occurs. This instant is recognized by a sudden or unusual change in the bit pattern. The tape is stopped there, rewound several inches, and replayed at 15/16th inches-per-second (1500 hertz) into a Honeywell Visicorder, Model 903C, light-beam oscillograph. The paper speed of the oscillograph is 50 inches-per-second. The resulting paper recording is a time-ordered duplicate of the original data signal. Since the basic data--photon count vs. time--is in digital form, the frequency response and driving speeds of the initial recording, playback recording and oscillograph recording need not be maintained to a critical tolerance. Under poor conditions the binary bit configuration retains its recognizability. Two

additional advantages of this type of recording are that the recorder can be left on for long periods of time, recording continuously even though the occultation itself occurs in only a few tenths of a second, and the data tape can be reused. A major disadvantage is that the data is not directly available in computer-readable format. Consequently, the binary numbers must be (tediously) converted by hand to their decimal equivalents and punched on cards for use in data analysis programs.

The dual-channel photometer, mounted on the Kitt Peak #2 36-inch telescope is pictured in Figure 3.4. The photomultiplier cooling chambers extend downward (channel 2) and to the left-rear (channel 1) from the photometer head. At the right-rear can be seen the d.c. amplifier--not used for occultation observations. Figure 3.5 shows the photon counter (center), the preamplifiers on the table in front of the counter, the stereo tape recorder, and a dual-trace oscilloscope used for real-time monitoring.

In order to investigate the effects of coincidence of pulses at the counter gate, assume that the pulse probability density function is  $p(x)$ . Then the probability that at any average pulse counting rate,  $X$ , there are rates less than or equal to a specific value,  $x$ , is  $F(x)$ , where

$$F(x) = \int_{-\infty}^x p(x) dx = P(X \leq x). \quad (3.2)$$

The observed pulse rate will be  $x_0 = XF(x)$ . If the pulse function,  $p(x)$ , can be described by a gaussian with center  $X$  and dispersion  $\sigma$ ,  $F(x)$  is

$$F(x; X, \sigma) = \frac{1}{\sigma\sqrt{2\pi}} \int_{-\infty}^x e^{-\frac{(u-X)^2}{2\sigma^2}} du. \quad (3.3)$$

Equation (3.3) can be expressed in terms of the normal probability integral (error function),  $\Psi_0(y)$ , as (Smirnov 1965)

$$1/2 + \Psi_0\left(\frac{x-X}{\sigma}\right). \quad (3.4)$$



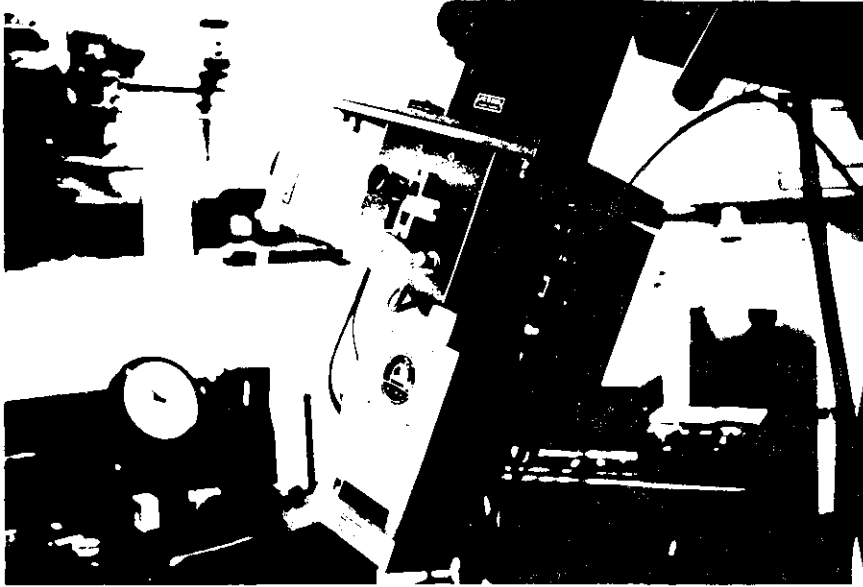


Fig. 3.4.--The Dual-channel Photometer

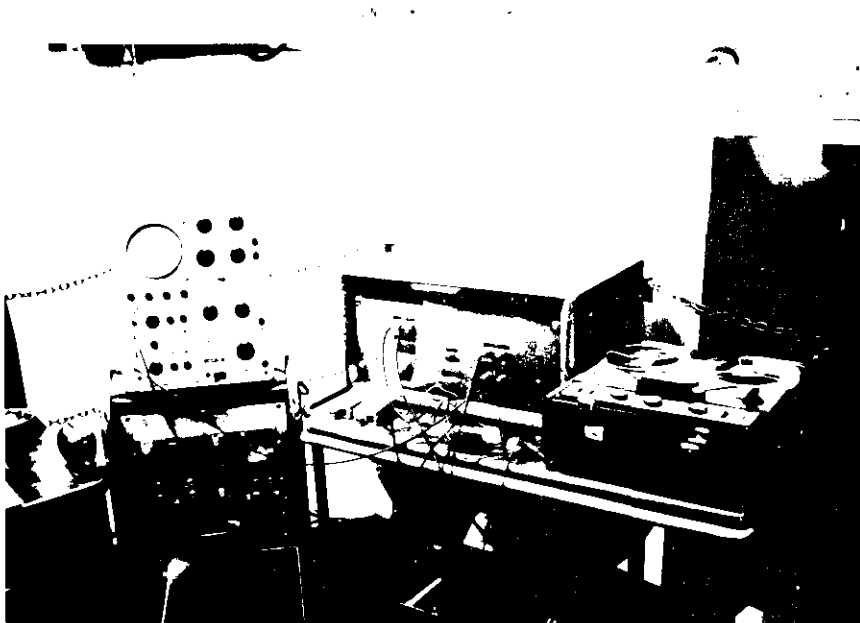


Fig. 3.5.--The Photon Counter and Accessories

Assuming that pulse coincidence is occurring at 2 Mhz.,  $x$  is set equal to 2 Mhz. If the "half-power" width of the gaussian describing the pulse arrival rate is the square root of the pulse rate, then the standard deviation,  $\sigma$ , is

$$\sigma = \sqrt{X/8 \ln 2} = .425\sqrt{X} \quad (3.5)$$

The distribution function is given by

$$F(2\text{Mhz}; X, 0.425\sqrt{X}) = 1/2 + \Psi_0 \left( \frac{2\text{Mhz} - X\text{Mhz}}{0.425\sqrt{X} \text{ Mhz}} \right). \quad (3.6)$$

Table 3.2 lists computed values of the distribution function, observed rates,  $x$ , and corrective multiplying factors for various true pulse rates,  $X$ .

TABLE 3.2

## Theoretical Coincident Pulse Rates

$X$	$F(x; X, \sigma)$	$x$	Correction
0.1 Mhz	1.0000	0.100 Mhz	1.00
0.4	1.0000	.400	1.00
0.7	0.9999	.700	1.00
1.0	.9909	0.991	1.01
1.4	.8830	1.238	1.13
1.7	.7064	1.201	1.41
2.0	.5000	1.000	2.00
2.5	.2284	0.565	4.37
3.0	.0869	.261	11.5
3.5	.0294	.103	34.0
4.0	.0092	0.037	109.

The curve  $X$  vs.  $x$  is double-valued--however only for the brightest stars observed through the broadest filters will rates exceeding one megahertz be encountered so that generally a corrective factor need not be applied. The dispersion described by equation (3.5) is probably broader than is actually found in practice since observations of bright stars show that pulse rates above 1.238 Mhz. can be encountered. For instance, the bright star  $\pi$  And,  $m_V = 4.36$  B5V, produced 1880 counts per integration cycle when observed with

the dual-channel photometer through the B filter. Such a rate is not predicted on the basis of Table 3.2. Possibly the definition of coincidence rate, 2 Mhz., is also low. In either case, the assumed estimates give worst-case results. Further remarks concerning the pulse counting capability of this instrument appear in Chapter 5.

## IV. Observations and Results

Occultation observations were made from two sites. For the December, 1967, occultations the Kitt Peak National Observatory's #2 36-inch telescope was used. All other observations were made on the 32-inch reflector at McCormick Observatory's Fan Mountain Station (Birney 1966).

The EMI photomultipliers were operated at 1100v DC overall for these observations. To reduce the brightness of the sky a focal plane diaphragm of diameter 0.71 mm. was always used. On the 32-inch Fan Mountain telescope the diaphragm admits a circle of light 11.3 seconds of arc in diameter, while this value is 11.9 seconds of arc for the Kitt Peak #2 36-inch. Table 4.1 lists the observed stars by their various catalog designations. The

TABLE 4.1

## Cross-identification List

DM	SAO	HR	GCRV	GC	HD	HII	Remarks
BD -18°6037	164756			30706	208482		
BD +23° 505	076126	1140	2077	4475	23288	447	Calaeno, 16 Tau
BD +23° 507	076131	1142	2079	4477	23302	468	Electra, 17 Tau
BD +23° 536	076192		2130	4536	23629	1375	24 Tau
BD +23° 540	076200		2137	4542	23642	1431	
BD +23° 541	076199	1165	2135	4541	23630	1432	Alcyone, 25 n Tau
BD +24° 547	076140	1145	2086	4486	23338	563	Taygeta, 19 Tau

column headed HII gives the Hertzsprung number for those stars of the Pleiades cluster (Hertzsprung 1947). All observed HII stars are Pleiades cluster members (Johnson and Mitchell 1958).

Of these seven stars, three were observed in two colors. Table 4.2a lists the occultation prediction parameters of each observation. The headings have the following meanings: DATE = the Julian Date of predicted disappearance - 2439000, DIST = the topocentric distance to the lunar limb in meters,  $v_r$  = the speed of the lunar limb in the direction normal to

the mean surface (edge) in seconds of arc per second, negative for disappearance, % = percent of the lunar disk illuminated, PA = position angle of event, measured from celestial north toward east in degrees, CA = the cusp angle, measured in degrees to the nearest (northern or southern) cusp, AA = the axis angle, measured in degrees, the argument needed to enter Watts' limb charts (Watts 1963) to obtain a limb profile, LIB $\lambda$  and LIB $\beta$  = the librations in longitude and latitude, measured in degrees, also needed for Watts' charts. Table 4.2b lists the occultation observation data. The filters are identified B,V,u,v,b,y and are described elsewhere in this paper. For the HII stars the apparent magnitudes, spectral types and color indices are taken from Mendoza (1956). PRE and POST are the average values of counts per integration cycle before and after the event. The error figures are r.m.s. values. The signal/noise is computed by taking PRE - POST and dividing by PREnoise.

The occultation figures themselves consist of two parts. In the lower section of the figure the table gives numbers of photons vs. time. The time interval always equals 1.04 milliseconds. The table should be read downwards in columns, then from left to right. The "star" beside one number indicates that that number is plotted at  $t = 0$  in the accompanying graph and approximates the time of geometric occultation. The graph in the upper section of the figure is a plot of photon "counts" vs. time. The photon counts (ordinate) are normalized to a 100% level for uniformity of presentation. The time axis (abscissa) is not normalized--each adjacent point is spaced at an equal 1.04 millisecond interval.

Table 4.3 is presented here to provide a framework within which the following discussions can be understood. For each star the table gives the blackbody (BB) value of stellar angular diameter, the restoration (R) derived value of stellar angular diameter plus mean error, and other perti-

TABLE 4.2a

## Occultation Prediction Data

NAME	DATE -2439000	DIST <sup>+</sup> 10 <sup>8</sup>	v <sub>r</sub>	%	PA	CA	AA	LIBA	LIBB
BD-18°6037	831.5791	3.852	-.3790	34	61	79N	80.1	6.87	6.44
BD+23° 505	1303.5485	3.959	-.3995	23	67	83N	78.9	2.17	-5.68
BD+23° 507	1303.5494	3.959	-.3653	23	108	56S	120.3	2.17	-5.68
BD+24° 547	1303.5729	3.967	-.1930	23	18	34N	30.1	2.10	-5.67
BD+23° 540	1303.6052	3.978	-.4690	23	87	78S	98.8	2.02	-5.64
BD+23° 536	1303.6076	3.978	-.3213	23	130	34S	142.2	2.02	-5.64
BD+23° 541	1303.6117	3.978	-.2915	23	135	29S	147.4	2.01	-5.63

TABLE 4.2b

## Occultation Observation Data

NAME	m <sub>v</sub>	SP	B-V	F	PRE	POST	S/N	FIG
BD-18°6037	6.6	A0		V	105±14	21±5	6.0	4.1
BD-18°6037	6.6	A0		B	151±16	21±5	8.1	4.2
BD+23° 505	5.23	B7IV	-0.12	B	225±35	20±4	5.9	4.3
BD+23° 507	3.59	B6III	-0.14	y	93±14	5±2	6.3	4.5
BD+24° 547	4.19	B6V	-0.14	V	230±40	20±4	5.3	4.7
BD+24° 547	4.19	B6V	-0.14	B	485±77	24±6	6.0	4.8
BD+23° 540	6.61	A0V	0.00	B	105±17	35±6	6.2	4.9
BD+23° 536	6.19	A0V	0.00	B	149±25	40±5	4.4	4.10
BD+23° 541	2.77	B7III	-0.12	b	245±65	5±2	3.7	4.12
BD+23° 541	2.77	B7III	-0.12	y	154±32	4±2	3.4	4.13

TABLE 4.3

## Observed Stellar Diameters

NAME	DIAM(BB)	DIAM(RD)	Remarks
BD-18°6037	0".00015	0".00179 (V) 0".00131 (B)	Effectively a point source
BD+23° 505	0".00020	0".00158	Diameter refers to primary; a definite double, separation = $0".0062 \pm 0".0002$ , in position angle $247^\circ$ ; $m = 2.0 \pm 0.2$
BD+23° 507	0".00040	0".00302 $\pm$ 0".00176	Diameter affected by secondary component; separation < $0".0025$ in pos. ang. $108^\circ$
BD+23° 536	0".00019	0".01040 $\pm$ 0".00171	Affected by lunar limb irregularities; detailed description in section H
BD+23° 540	0".00015	0".00207	Secondary component not seen in pos. ang. $87^\circ$
BD+23° 541	0".00063	0".00164 (b) 0".00222 (y)	This star not double; data very noisy
BD+24° 547	0".00030	0".00187 (V) 0".00195 (B)	Cannot confirm duplicity of this spectroscopic binary

nent remarks. Those restoration diameters without mean error represent upper limits. The blackbody diameter is computed by comparison with the solar luminosity (Allen 1963, pg. 191) from

$$\log D'' = 5.43812 - \frac{BC}{5} - \frac{m_V}{5} - 2 \log T_e. \quad (4.1)$$

Values of the bolometric correction, BC, and effective temperature,  $T_e$ , are taken from Morton and Adams (1968).

In essence Table 4.3 is a summary of and represents the results of the present investigation. A detailed discussion of each observation and its interpretation is given on the following pages. Each occultation is taken up in turn. A standard presentation format is used throughout. On the first page the upper lines give data of astrophysical importance. The restoration limits are computed from equations (2.15-19) using the observed parameters. The table lists the following observed or computed quantities:  $b_r$  = the restoring beamwidth,  $b_1$  = the half-power width of the gaussian fit to the restored curve,  $S/N_r$  = r.m.s. signal/noise of the restored curve,  $F$  = the relative stellar flux = the area of the gaussian curve,  $\Delta b_1$  = the estimated error of  $b_1$ ,  $A_1$  = the computed square of the diameter,  $\Delta A_1$  = the mean error of  $A_1$ , and  $w_1$  = the weight. The line following the table is the weighted mean square of the diameter,  $A$ , and the weighted mean error,  $D$ . Signed suffixes indicate the appropriate power of ten, e.g.  $1.234-5 = 1.234 \times 10^{-5}$ . If  $X = A/D > 1$ , the diameter and mean error are computed by equation (2.22); otherwise the upper limit of the diameter is given by equation (2.23). The second page illustrates the occultation curve and digital data as previously described. The third page, when included, shows restored curves for each restoring beamwidth. The abscissa is in thousandths of a second of arc and the ordinate is arbitrary. The restoring beamwidth is indicated at the side of each curve.



A. BD -18°6037 (V color)

$m_V = 6.6$  A0, B.C. = -0.17,  $T_e = 9600^\circ$

Computed blackbody diameter = 0".00015

Restoration limits:  $R_N = .00028$ ,  $R_A = .00032$ ,  $R_L = .00153$ ,  $R_T = .00039$

$S/N_0 = 6.0$

TABLE 4.4

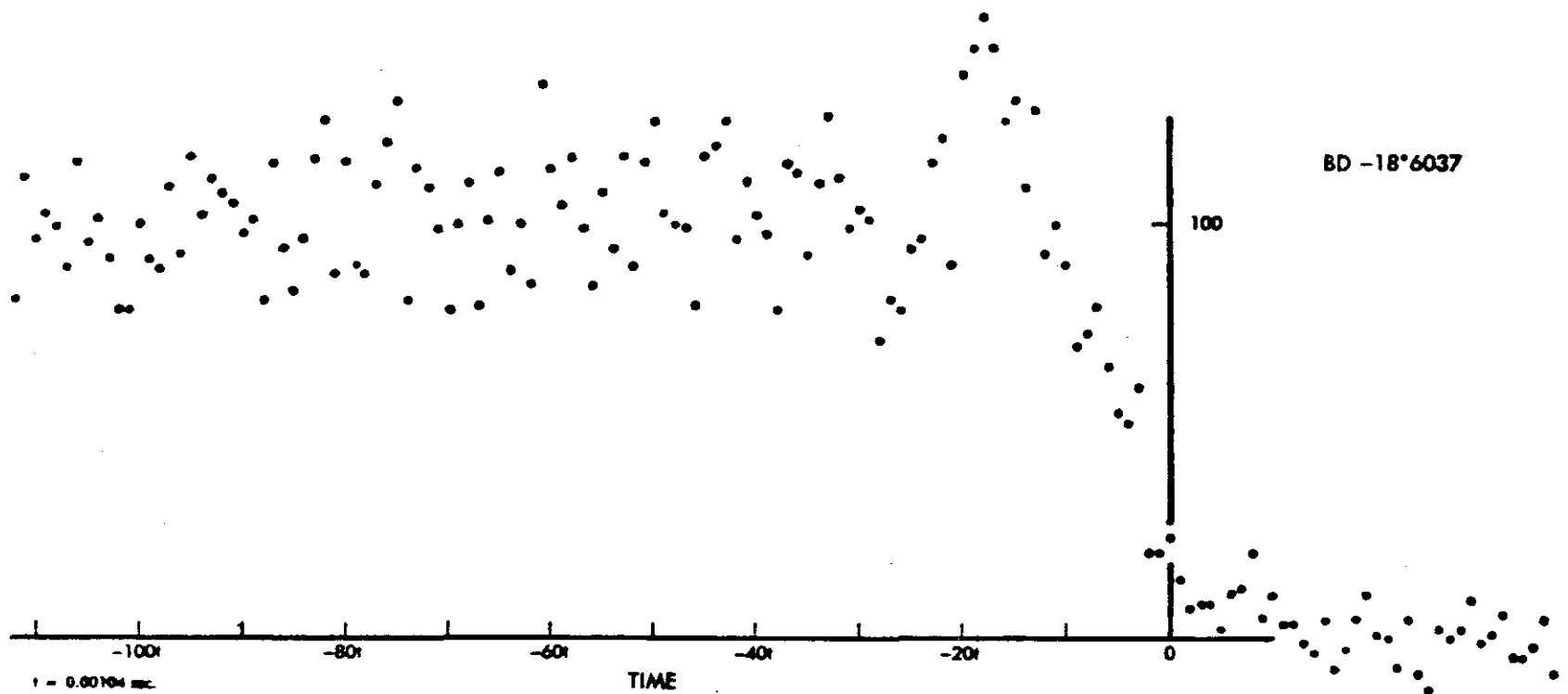
Restoration Data

$b_r$	$b_l$	$S/N_r$	F	$\Delta b_l$	$A_l$	$\Delta A_l$	$w_l$
.025598	.0253529		85	.0010480	-1.358-5	5.317-5	0.035+10
.019436	.0194433		85	.0009223	-1.617-6	3.586-5	0.077+10
.008533	.0087817	20.	86	.0006291	3.910-6	1.104-5	0.819+10
.006488	.0066496	17.	84	.0005463	1.824-6	7.265-6	1.894+10
.004266	.0046944	13.	85	.0004756	3.612-6	4.465-6	5.014+10
.003244	.0037750	12.	86	.0004386	3.534-6	3.311-6	9.118+10
.002560	.0029893	10.	82	.0003909	2.229-6	2.337-6	18.30+10
.001946	.0022233	8.5	75	.0003335	1.044-6	1.483-6	45.46+10
.001707	.0019597	7.5	72	.0003138	8.280-7	1.230-6	66.06+10

$A = 1.358-6$ ,  $D = 1.850-6$ ,  $X = .734$

diameter = 0".00179

This star appears to be a star of the pointsource variety. Beyond basic classification there is little observational history to this star, and there is no hint of any peculiarity. Restorations of model pointsource occultation curves with  $S/N_0 = 6$  yield upper limits of the same order of magnitude as the upper limit for the diameter found here. Combining the data of the two color curves, the weighted upper limit to the diameter is 0".00155. The ratio of observed fluxes,  $F_V/F_B$ , is 0.645. The stellar fluxes should be roughly the same for this A0 star in the two wavelengths. That the observed flux ratio is not unity is the result of the different relative response of the photometer in the two bandpasses.



34

93	92	103	107	98	99	86	94	115	87	102	89	87	21	18	25	28	18	19	17
91	103	105	108	98	102	101	115	98	104	87	86	75	19	18	24	18	24	25	21
106	128	99	102	117	102	118	99	90	113	116	98	66	26	20	22	25	25	25	23
104	79	115	108	110	88	101	104	100	94	118	102	64	16	26	21	20	17	29	11
116	89	106	86	116	102	101	96	116	103	123	115	71	20	15	27	21	26	21	19
98	97	120	109	104	120	91	86	123	91	100	120	39	26	19	16	30	22	27	15
99	97	107	89	105	119	101	86	93	130	111	95	39	31	30	19	18	30	18	21
89	97	94	97	117	112	109	103	115	114	105	132	42★	23	15	25	19	19	23	17
108	126	106	78	100	107	105	96	95	107	101	137	34	22	25	31	17	23	13	15
104	83	97	93	104	103	103	94	93	116	86	143	28	16	12	21	24	21	12	10
104	98	99	108	95	109	92	110	111	102	115	137	29	26	27	21	20	19	21	32
114	98	95	97	90	121	96	97	119	91	113	123	29	15	16	24	23	13	25	14
116	115	85	109	96	103	126	116	127	109	97	127	24	12	19	28	16	15	25	23
113	95	105	101	123	102	97	105	88	98	111	110	31	24	18	15	22	17	22	23
102	101	96	127	105	119	107	112	114	116	124	125	32	22	14	20	17	21	21	23
100	127	99	115	95	102	88	109	110	95	112	97	39	24	22	19	21	15	21	23
99	92	116	95	95	101	112	107	102	115	102	103	26	30	24	34	29	14	26	24
111	105	127	101	111	127	100	101	86	123	106	95	31	21	21	17	24	24	25	26
103	105	108	111	119	91	105	104	103	105	104	79	25	23	20	25	23	29	24	22
62	85	89	103	84	122	102	88	111	103	80	82	25	27	22	31	26	19	17	21

FIGURE 4.1.-- PHOTON COUNT vs TIME

B. BD -18°6037 (B color)

$m_v = 6.6$  A0, B.C. = -0.17,  $T_e = 9600^\circ$

Computed blackbody diameter = 0".00015

Restoration limits:  $R_N = .00028$ ,  $R_A = .00032$ ,  $R_L = .00195$ ,  $R_T = .00039$  \*

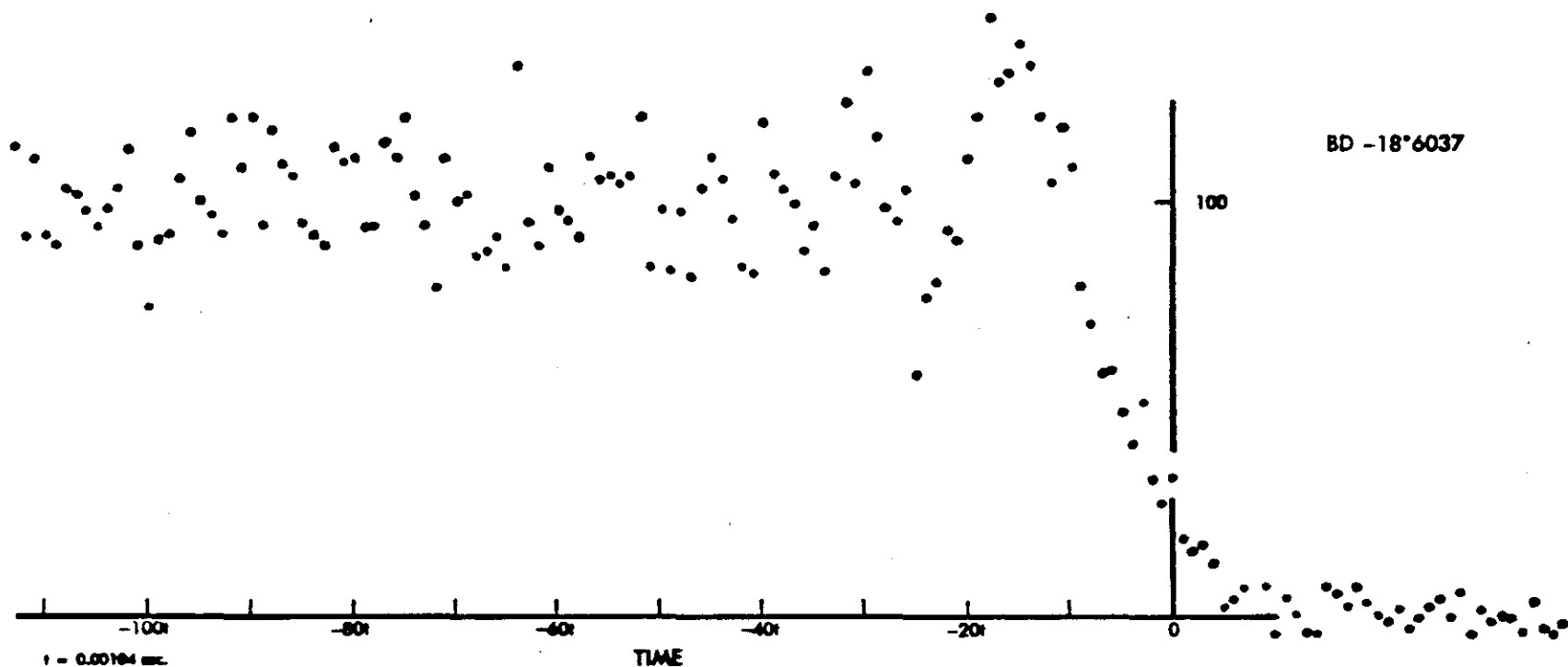
$S/N_o = 8.1$

TABLE 4.5

Restoration Data

$b_r$	$b_l$	$S/N_r$	F	$\Delta b_l$	$A_l$	$\Delta A_l$	$w_l$
.023062	.0229462		128	.0007407	-5.876-6	3.399-5	0.087+10
.017535	.0173630		126	.0006427	-6.415-6	2.232-5	0.201+10
.007687	.0079637	22.	131	.0004452	4.132-6	7.091-6	1.988+10
.005845	.0059255	20.	127	.0003799	8.031-7	4.502-6	4.932+10
.003844	.0036895	16.	123	.0002917	-1.249-6	2.152-6	21.58+10
.002923	.0028661	11.	126	.0002598	-3.969-7	1.489-6	45.06+10
.002306	.0023932	10.	129	.0002442	3.491-7	1.169-6	73.15+10
A = -6.067-8, D = 1.652-6, X = -.036							
diameter = 0".00131							

Restorations of this occultation curve indicate no unusual characteristics, confirming the V color observation.



36

177	147	147	133	146	149	156	151	161	134	126	143	96	16	20	36	15	25	13	16
156	139	143	147	156	157	125	146	157	138	153	153	97	15	16	32	35	26	22	21
143	138	147	150	175	147	159	141	143	129	163	95	84	30	25	24	31	27	23	16
132	155	160	151	151	141	175	147	139	191	156	119	74	28	17	23	14	23	22	21
141	159	175	159	160	137	145	153	136	143	144	124	87	24	15	22	22	15	20	24
156	137	146	146	148	175	148	165	166	135	129	140	63	30	18	20	30	20	22	22
151	139	139	174	161	153	161	136	161	160	127	137	56	25	21	25	19	18	18	25
161	147	144	138	160	146	145	116	163	147	173	162	64★	21	20	17	23	15	21	23
154	161	159	141	145	153	131	137	141	143	158	175	45	19	24	16	22	16	27	18
161	161	143	139	167	147	139	139	141	138	153	206	41	23	12	21	19	23	24	19
136	155	153	152	135	143	143	156	167	163	148	184	43	17	27	15	30	18	28	18
143	161	138	151	159	151	135	170	163	156	134	189	37	20	14	25	18	20	20	22
128	146	164	155	152	158	130	149	175	157	142	198	25	24	22	21	29	19	29	26
147	160	161	146	127	160	153	145	151	155	127	191	26	26	22	22	20	18	27	25
137	151	150	141	135	162	166	139	142	157	157	176	31	20	16	21	15	15	27	24
141	166	140	155	163	145	136	175	122	175	180	155	62	28	25	19	22	22	13	17
142	150	147	163	143	155	162	160	162	129	155	172	30	15	18	21	25	20	26	27
163	159	163	166	155	144	139	175	149	147	189	160	15	23	20	12	23	17	21	22
145	130	141	172	144	153	136	142	151	128	169	123	27	19	25	25	21	14	22	16
165	143	149	139	150	139	153	171	132	146	147	111	21	21	24	23	21	22	16	22

FIGURE 4.2.-- PHOTON COUNT vs TIME

C. BD +23° 505 (B color)

$m_V = 5.23$  B7IV, B.C. = -0.91,  $T_e = 13600^\circ$

Computed blackbody diameter = 0".00020

Restoration limits:  $R_N = ".00054$ ,  $R_A = ".00029$ ,  $R_L = ".00195$ ,  $R_T = ".00042$  \*

$S/N_0 = 5.9$

TABLE 4.6

Restoration Data

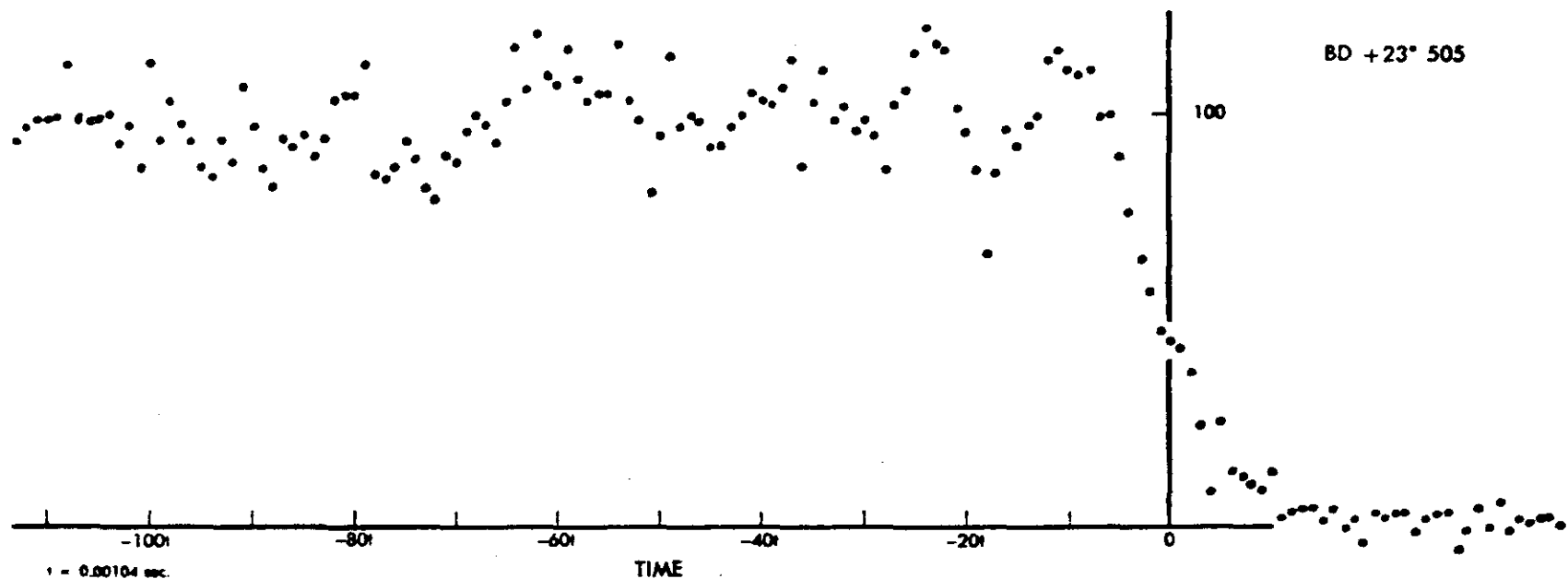
$b_r$	$b_l$	$S/N_r$	$F$	$\Delta b_l$	$A_l$	$\Delta A_l$	$w_l$
".003791	".0039438	6.5	154	".0004425	9.860-7	3.490-6	8.205+10
.002883	.0029274	5.5	147	.0003767	1.160-7	2.205-6	20.55+10
.002275	.0024025	5.0	145	.0003480	4.752-7	1.672-6	35.75+10
A = 4.258-7, D = 2.074-6, X = .205 diameter = 0".00158							

As illustrated in Figure 4.4, restorations with narrowing beamwidths quickly reveal the secondary component at separation  $0".0062 \pm 0".0002$  in scan position angle  $247^\circ$ . The position angle refers to the separation in the direction normal to the lunar limb at the time of occultation. The upper limit for the diameter given above refers to the primary component of this newly detected binary system. A comparison of the areas under the restored curves of each component gives a  $\Delta m_B = 2.0 \pm 0.2$ . An approximate period for the system of 0.25 years is derived by assuming that the mass-luminosity law holds and the mass of the primary is about  $5 M_\odot$  (Allen 1963, pg. 203), the system is 126 parsecs distant (Johnson 1968), and  $0".0062$  is the semi-major axis of the orbit.

Abt, Barnes, Biggs, and Osmer (1965) see no unusual radial velocity variations which might suggest duplicity, but low orbital inclination, large

$\Delta m$ , or a data selection effect might preclude detection of the secondary from those measurements. Abt's criterion for detection is that "the scatter in the velocity measures appreciably exceeds the mean internal probable error.." Their mean internal error for this star is 5.6 km./sec. Using the above assumed values for  $a$  and  $P$ , the true velocity in a circular orbit is about 90 km./sec. Their range of measured velocities ("range" and "scatter" do not have the same definition) is +16 km./sec. to -14 km./sec., or  $\pm 15$  km./sec. If this range is at the limit of detectability, the true orbital inclination must be less than  $10^\circ$ .

Figure 4.4a is a plot of Abt's (et. al.) observed radial velocities with probable error bars vs. phase, where the assumed period is 90 days and the epoch is arbitrary. The reader is referred to the original paper for tabulated values of dates and radial velocities. The curve is shown only to indicate the interesting possibilities that further investigation of this system hold. There is no a priori reason for expecting the measured scan separation to equal the semi-major axis. For the present these calculations are only to be regarded as interesting diversions. Careful future observations of this star--spectroscopic, photoelectric, and occultation--can reveal more definitive results.



39

223	248	211	195	195	200	183	199	194	242	226	236	228	220	114	12	18	20	12	17
261	203	216	173	203	191	183	213	213	205	227	231	224	210	109★	25	24	19	13	24
224	236	214	183	191	199	182	213	189	223	241	249	221	191	106	24	15	18	20	23
258	231	235	170	208	171	161	187	191	213	189	235	230	151	94	25	10	17	22	22
227	242	197	184	184	172	152	209	172	204	186	224	244	190	69	25	17	15	20	17
222	214	203	179	201	184	167	217	206	191	192	227	193	210	37	17	22	15	21	19
223	211	185	193	199	174	184	239	211	187	205	227	223	203	70	23	16	16	23	25
202	214	198	183	207	191	207	205	205	205	196	251	239	213	46	25	24	28	18	19
211	219	223	194	200	156	171	188	211	194	182	224	214	215	43	25	25	26	24	19
206	193	179	199	216	187	178	198	215	229	177	215	221	243	40	9	23	17	14	12
217	201	204	203	215	187	199	200	215	211	198	180	210	248	37	13	18	15	16	24
207	208	178	198	215	160	218	219	216	191	194	206	215	239	46	28	19	29	21	14
233	181	178	237	184	185	191	200	241	183	210	245	208	237	24	19	18	18	24	14
223	207	206	205	203	180	223	214	215	205	217	211	191	239	27	31	24	20	15	17
243	192	186	210	193	174	191	207	214	201	212	217	222	216	28	17	20	20	19	18
232	191	189	223	191	184	214	214	215	207	204	214	229	217	28	23	24	24	13	16
251	188	179	203	206	203	202	201	217	230	223	202	247	197	22	21	21	14	17	16
255	232	162	215	186	185	183	195	203	197	250	203	259	171	28	23	17	13	20	18
220	183	191	244	190	204	208	203	212	206	230	212	251	148	18	24	21	25	21	14
249	222	202	177	227	173	213	188	191	224	256	218	248	132	23	20	23	22	17	19

FIGURE 4.3.-- PHOTON COUNT vs TIME

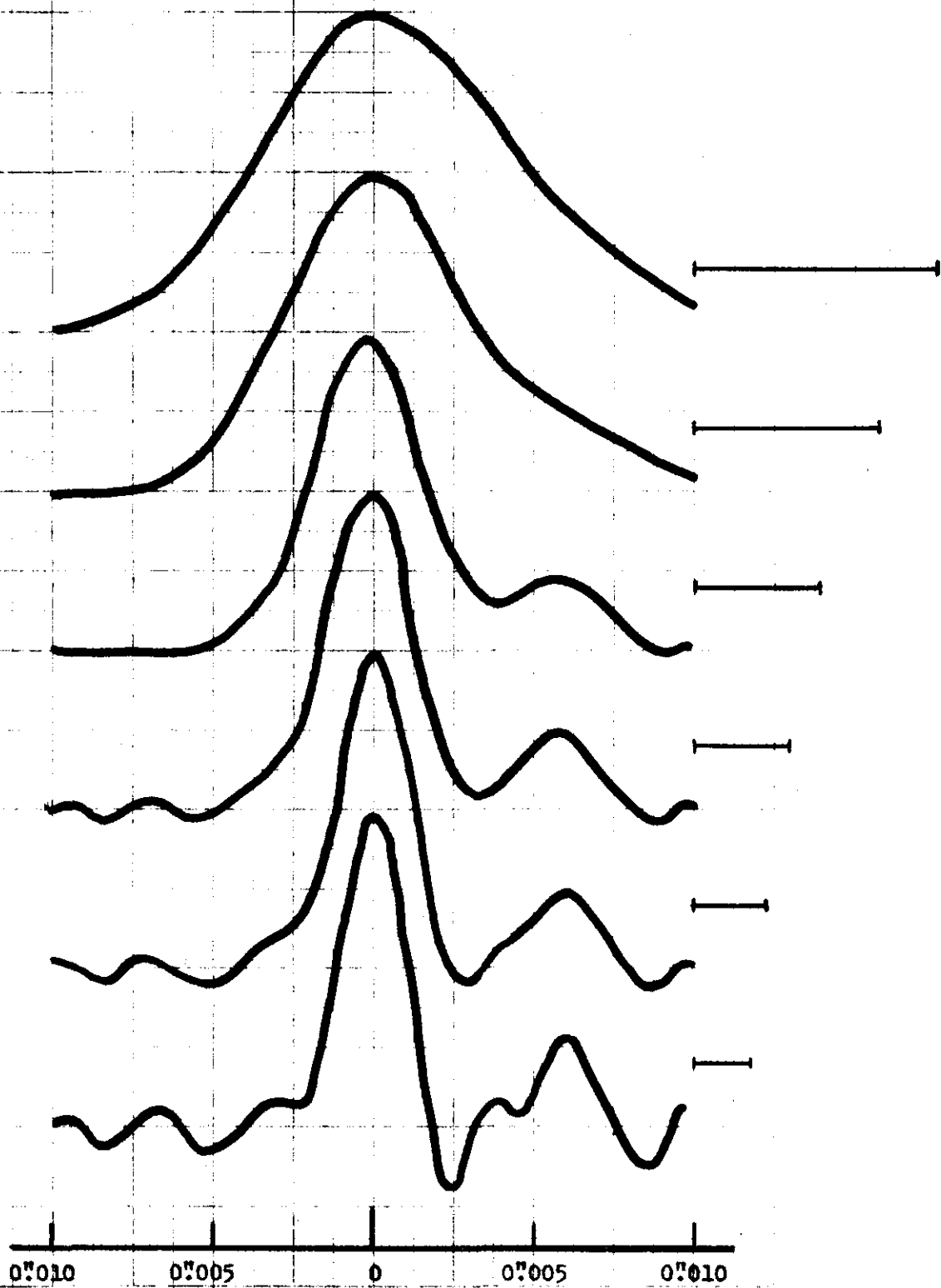


Fig. 4.4.--Restoration Curves for BD +23°505



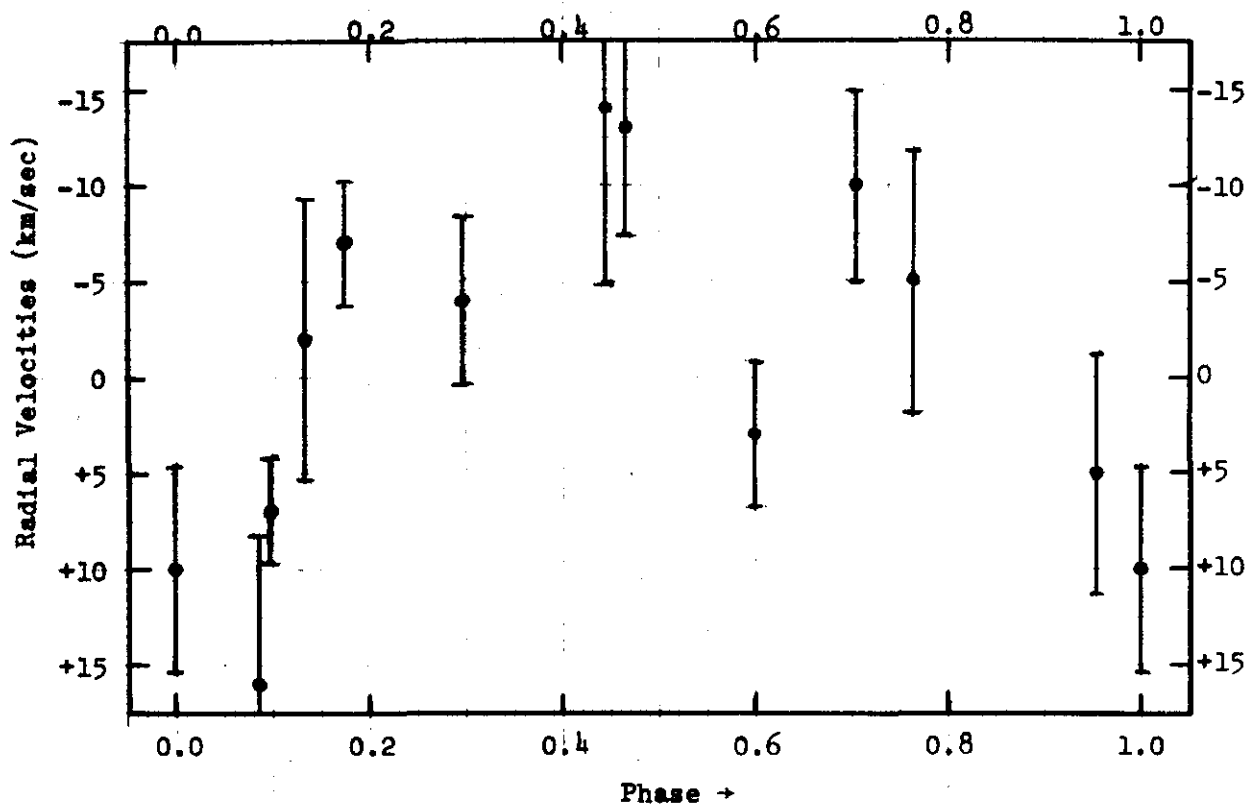


Fig. 4.4a.--Radial Velocities vs. Phase (P = 90 days)

## D. BD +23° 507 (y color)

$m_v = 3.59$  B6III, B.C. = -1.05,  $T_e = 14600^\circ$

Computed blackbody diameter = 0".00040

Restoration limits:  $R_N = .00050$ ,  $R_A = .00029$ ,  $R_L = .00096$ ,  $R_T = .00038$

$S/N_0 = 6.3$

TABLE 4.7

Restoration Data

$b_r$	$b_l$	$S/N_r$	F	$\Delta b_l$	$A_l$	$\Delta A_l$	$w_l$
.025203	.0261769		96	.0010200	4.899-5	5.341-5	0.035+10
.019163	.0202824		94	.0009066	4.333-5	3.677-5	0.074+10
.008401	.0092578	16.	89	.0006249	1.473-5	1.157-5	0.747+10
.006388	.0071158	10.	83	.0005508	9.524-6	7.840-6	1.626+10
.004201	.0050020	6.0	83	.0004775	7.143-6	4.777-6	4.381+10
A = 9.138-6, D = 6.835-6, X = 1.337							
diameter = 0".00302 $\pm$ 0".00176							

This star is a known spectroscopic binary (Abt, et. al., op. cit.) with the following elements:  $P = 100.46$  days,  $T = \text{JD } 2424472.86$ ,  $\omega = 0$ ,  $e = 0.522$ ,  $K = 26.0$  km./sec.,  $\gamma = -0.3$  km./sec.,  $a \sin i = 30.64 \times 10^6$  km., and  $f(M) = 0.114$ . Although somewhat noisier, the observed occultation curve resembles the curve for BD +23° 505 in that the first two fringes are of about equal amplitude. Restoration at the resolution limit shows the unusual behavior of the intensity profile for this binary, Figure 4.6. The computed diameter is undoubtedly affected by the presence of the secondary component which is  $< 0".0025$  in scan position angle  $108^\circ$ . Using the spectroscopic elements and a distance to the Pleiades of 126 parsecs (Johnson 1968), the separation of the components is  $\rho'' = .00243 \sqrt{(1 - .0365 \sin^2 i) / \sin^2 i}$ . (This computation is discussed fully in Chapter 5.)

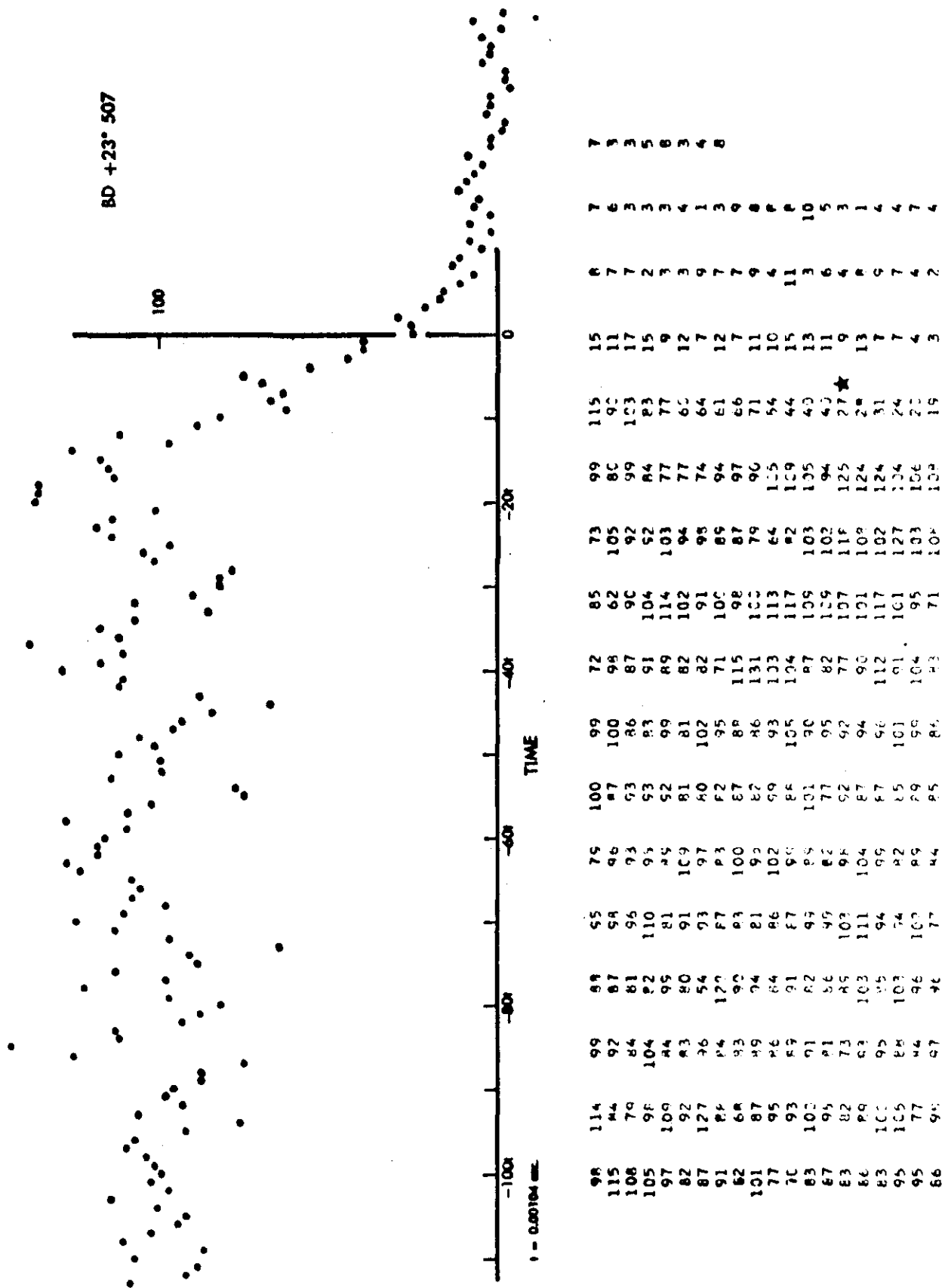


FIGURE 4.5.-- PHOTON COUNT VS TIME

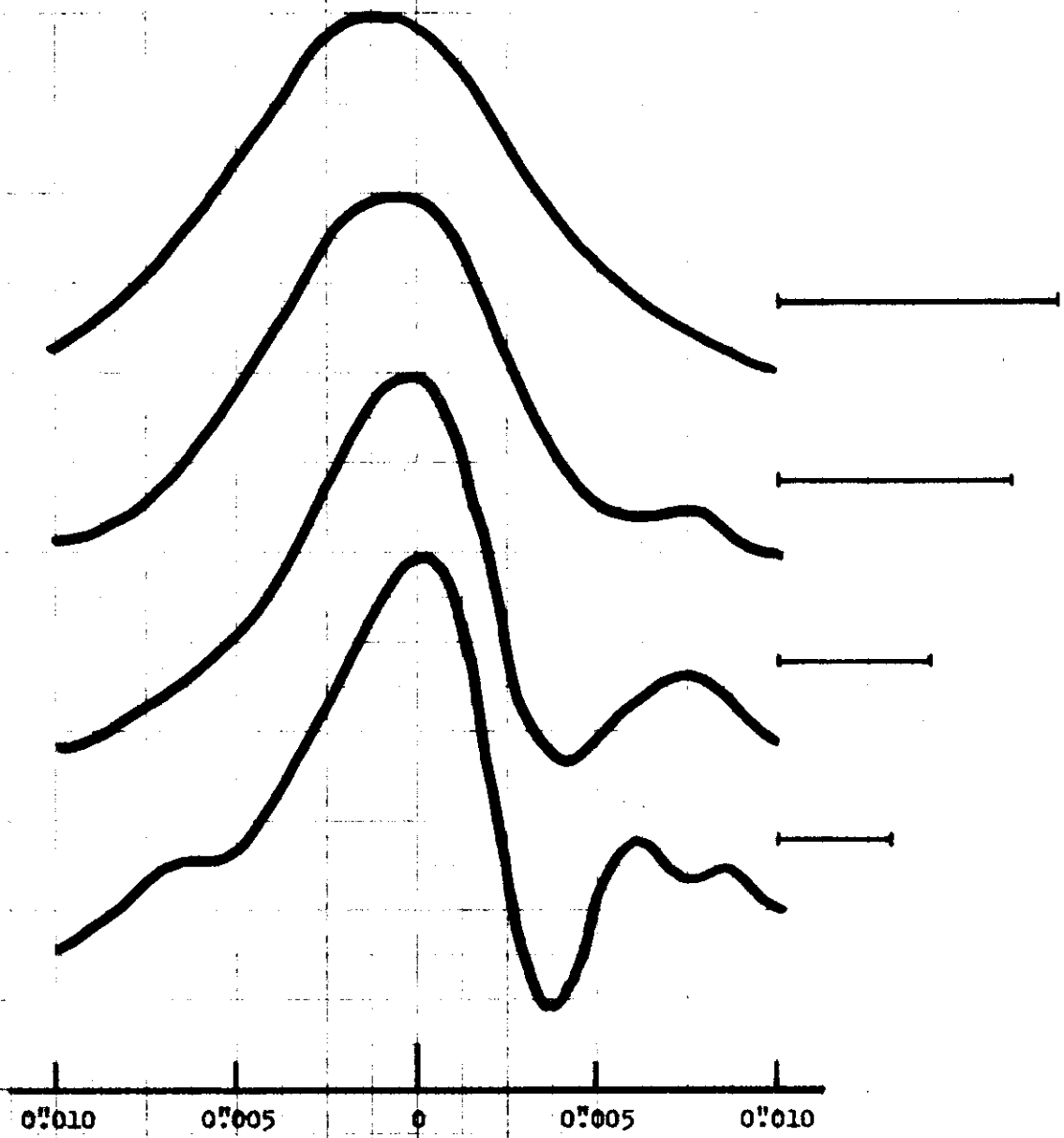


Fig. 4.6.—Restoration Curves for BD +23°507

E. BD +24° 547 (V color)

$m_V = 4.19$  B6V, B.C. = -1.05,  $T_e = 14600^\circ$

Computed blackbody diameter = 0".00030

Restoration limits:  $R_N = ".00043$ ,  $R_A = ".00029$ ,  $R_L = ".00153$ ,  $R_T = ".00020$  \*

$S/N_0 = 5.3$

TABLE 4.8

Restoration Data

$b_r$	$b_l$	$S/N_r$	F	$\Delta b_l$	$A_l$	$\Delta A_l$	$w_l$
".008408	".0080558		177	".0005022	-6.050-6	8.092-6	1.527+10
.006393	.0060264		180	.0004309	-4.738-6	5.193-6	3.707+10
.004204	.0039859		189	.0003514	-1.909-6	2.801-6	12.73+10
.003197	.0033160		201	.0003352	6.626-7	2.223-6	20.22+10
.002522	.0028947	6.5	211	.0003295	1.910-6	1.907-6	27.47+10
.001918	.0026915	4.8	246	.0003513	3.442-6	1.891-6	27.95+10
A = 1.185-6, D = 2.324-6, X = .510							
diameter = 0".00187							

Taygeta is a known spectroscopic binary with the following elements

(Abt, et. al., op. cit.):  $P = 1313$  days,  $T = \text{JD } 2423268.4$ ,  $\omega = 279^\circ.9$ ,  $e = .073$ ,

$K = 8.0$  km./sec.,  $\gamma = +5.9$  km./sec.,  $a \sin i = 144 \times 10^6$  km., and  $f(M) = .069$ .

Restorations of this occultation curve do not indicate the presence of the

secondary component, but set an upper limit to the diameter of 0".0019. The

separation of the components is  $\rho'' = \frac{.00709}{\sin i} \sqrt{1 - .9997 \sin^2 i}$ . That no component

is seen may be indicative of either a high orbital inclination, in which case

the predicted separation of the components would be very small, or unfavorable

scan position angle; the effects cannot be separated with this single obser-

vation. If the inclination of the orbit is low, the true position angle is

about  $292^\circ$ ; but if the separation is actually less than 0".0015 the inclination

is greater than  $80^\circ$ .

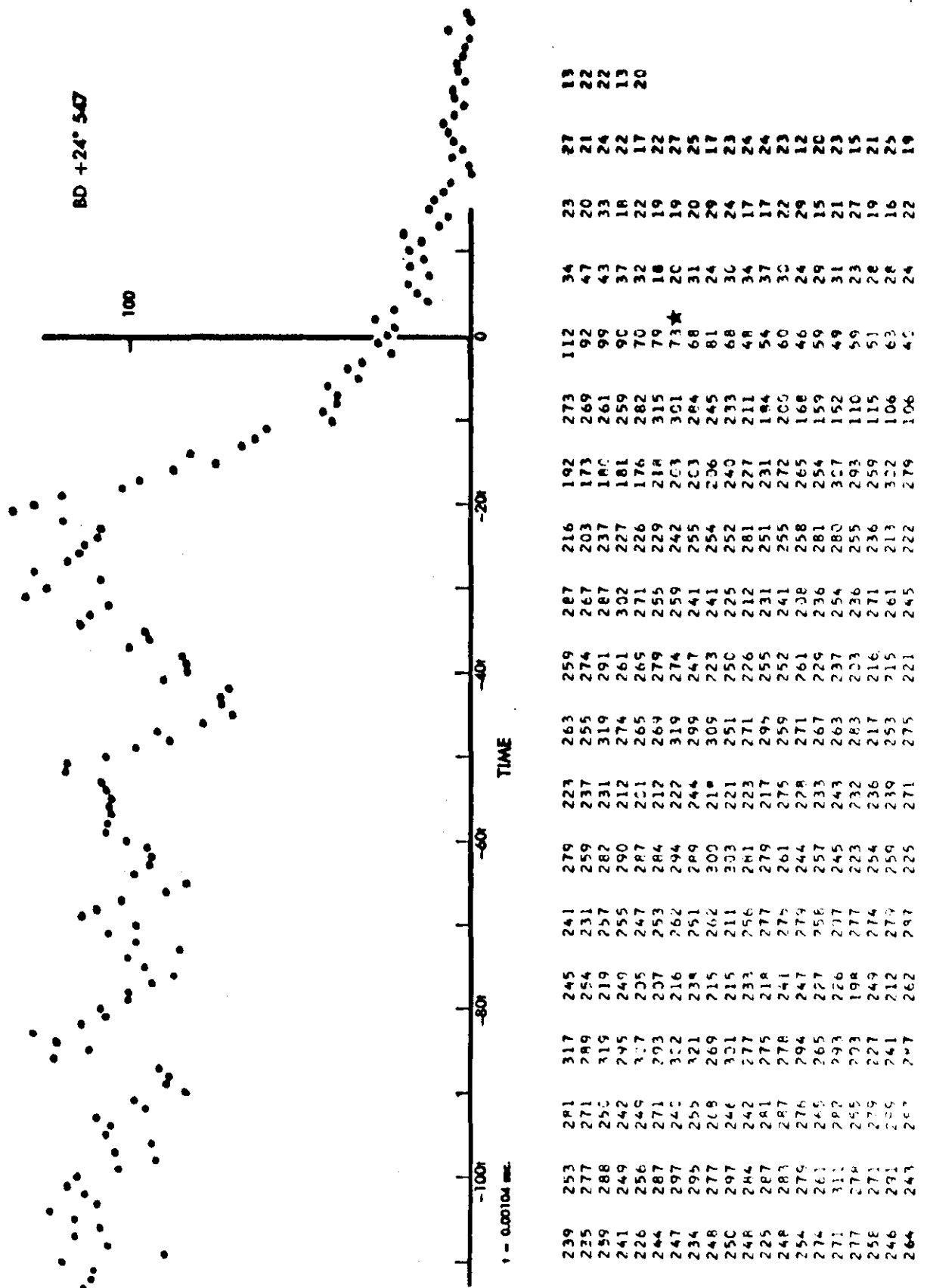


FIGURE 4.7.--- PHOTON COUNT vs TIME

F. BD +24° 547 (B color)

$m_V = 4.19$  B6V, B.C. = -1.05,  $T_e = 14600^\circ$

Computed blackbody diameter = 0".00030

Restoration limits:  $R_N = .00033$ ,  $R_A = .00029$ ,  $R_L = .00195$ ,  $R_T = .00020$  \*

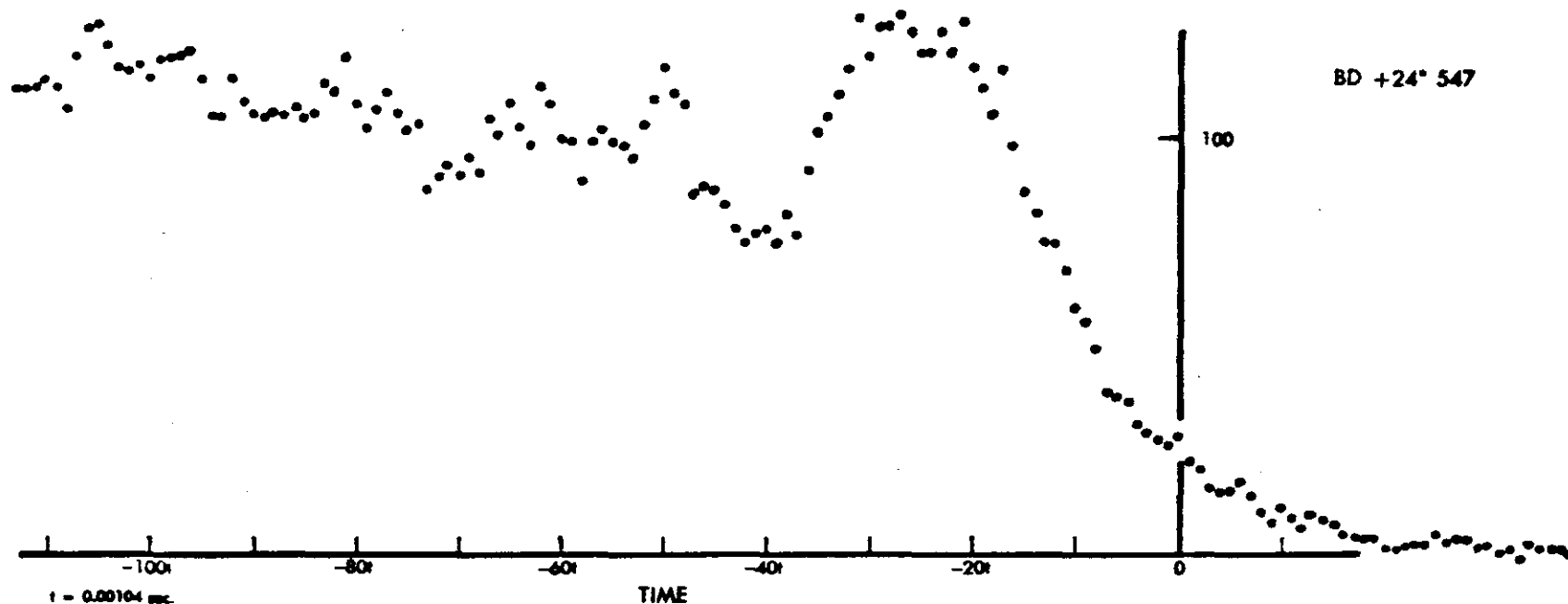
$S/N_0 = 6.0$

TABLE 4.9

Restoration Data

$b_r$	$b_l$	$S/N_r$	F	$\Delta b_l$	$A_l$	$\Delta A_l$	$w_l$
.007575	.0066510	11.	365	.0003859	-1.329-5	5.133-6	3.794+10
.005760	.0053726	9.5	411	.0003574	-4.440-6	3.841-6	6.776+10
.003788	.0039350	8.5	460	.0003228	1.013-6	2.541-6	15.48+10
.002880	.0033231	7.5	480	.0003127	2.650-6	2.078-6	23.15+10
.002273	.0030579	7.0	531	.0003239	4.079-6	1.980-6	25.48+10
A = 1.349-6, D = 2.456-6, X = .549							
diameter = 0".00195							

Restorations of this occultation curve confirm the V-color observation, and they do not indicate the secondary component. Combining both-color restorations, the weighted mean upper limit of the diameter is 0".00191. The near-grazing circumstance of this occultation allows a comparison of the predicted fringe frequency and the observed fringe frequency to be made for the purpose of finding a lunar slope. The lunar slope at the point of disappearance is found to be  $4.1 \pm 0.1$  (see Chapter 5 for a more detailed discussion of this computation). The correct value of lunar limb speed,  $v_r = -.2207$  "/second, has been used in all calculations.



461	575	622	607	531	514	566	510	469	575	511	509	427	623	208	73	39	39
472	625	555	665	543	472	557	471	509	607	519	491	435	605	203	67	41	29
485	632	595	691	541	495	582	511	509	611	510	527	431	580	199	61	35	33
511	569	623	479	541	490	569	509	494	589	515	499	414	584	174	51	35	29
479	571	583	704	459	551	501	459	539	563	549	479	387	603	163	49	35	30
511	555	543	651	509	535	525	475	527	561	539	545	371	583	157	47	29	
471	573	566	664	474	535	557	486	576	567	575	523	383	616	152	47	35	
475	575	543	603	499	511	543	479	607	551	524	467	386	566	160★	37	36	
469	590	535	647	527	511	582	485	579	573	497	483	373	543	133	35	33	
477	601	527	675	477	591	575	487	575	575	519	440	403	515	123	39	19	
487	599	527	654	525	511	541	497	596	578	479	483	381	563	101	40	33	
519	643	565	632	529	545	535	460	528	584	513	495	452	478	97	40	23	
521	655	543	603	509	545	631	485	599	551	495	483	494	426	99	52	38	
527	631	677	614	511	575	554	466	599	511	503	479	511	405	109	42	34	
536	618	596	710	527	501	570	507	542	511	431	465	535	373	95	46	33	
551	607	548	607	538	599	543	511	541	551	447	501	563	371	74	44	23	
543	623	565	619	519	615	615	460	543	527	456	529	619	341	65	37	28	
571	622	567	554	543	637	567	487	551	513	448	565	577	303	81	38	30	
588	596	585	591	553	575	561	482	542	510	467	534	611	286	68	29	32	
615	607	621	575	476	639	511	497	518	515	450	525	612	255	59	32	31	

FIGURE 4.8.-- PHOTON COUNT vs TIME



G. BD +23° 540 (B color)

$m_V = 6.61$  AOV, B.C. = -0.17,  $T_e = 9600^\circ$

Computed blackbody diameter = 0".00015

Restoration limits:  $R_N = .00066$ ,  $R_A = .00029$ ,  $R_L = .00195$ ,  $R_T = .00049$

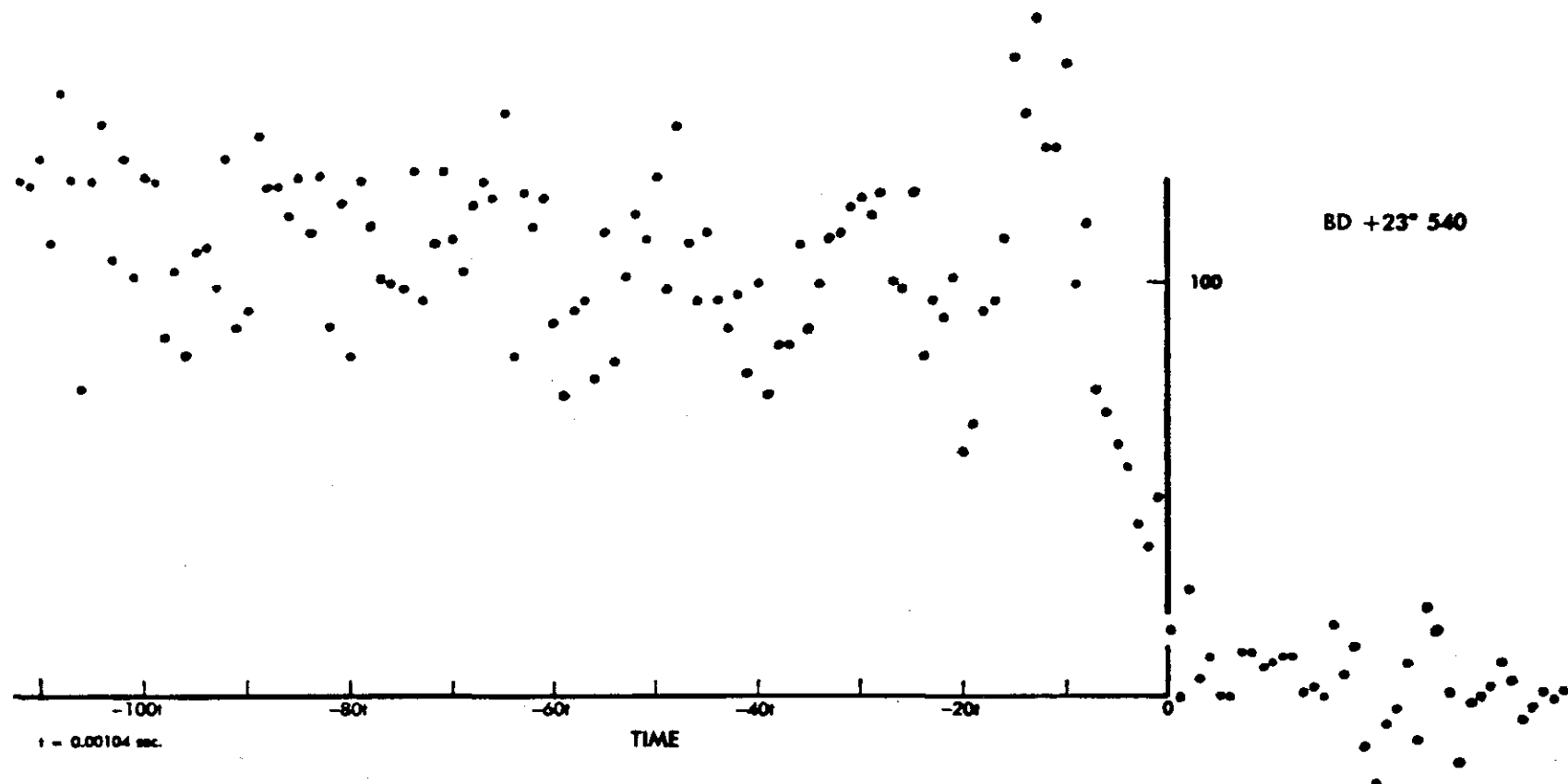
$S/N_o = 6.2$

TABLE 4.10

Restoration Data

$b_r$	$b_l$	$S/N_r$	F	$\Delta b_l$	$A_l$	$\Delta A_l$	$w_l$
.022694	.0245338		81	.0011600	8.554-5	5.693-5	0.031+10
.017255	.0161240		69	.0008744	-3.851-5	2.820-5	0.126+10
.007565	.0069581	11.	75	.0005699	-9.138-6	7.931-6	1.589+10
.005752	.0051745	8.5	78	.0004860	-6.546-6	5.030-6	3.951+10
.003782	.0036245	6.0	83	.0004198	-1.342-6	3.043-6	10.79+10
.002876	.0033799	5.5	100	.0004489	2.950-6	3.035-6	10.85+10
.002269	.0031867	5.0	111	.0004766	4.779-6	3.037-6	10.83+10
A = 6.999-7, D = 3.575-6, X = .196							
diameter = 0".00207							

This star is a known double-line spectroscopic binary (Abt, et. al., op. cit.) with these elements:  $P = 2.46113$  days,  $T = \text{JD } 2403104.408$ ,  $\omega = 107^\circ.7$ ,  $e = .018$ ,  $K_1 = 98.1$  km./sec.,  $K_2 = 140.6$  km./sec.,  $\gamma = +4.99$  km./sec.,  $a_1 \sin i = 3.32 \times 10^6$  km.,  $a_2 \sin i = 4.76 \times 10^6$  km.,  $M_1 \sin^3 i = 2.05$ , and  $M_2 \sin^3 i = 1.43$ . Restorations place an upper limit to the diameter of 0".0021 and do not indicate the secondary component in scan position angle  $87^\circ$ . The predicted angular separation of the components is  $\rho'' = \frac{.00043}{\sin i} \sqrt{1 - .0226 \sin^2 i}$ . Thus only for a very low inclination orbit would one expect the secondary to be discerned at this time.



94	109	92	117	88	128	95	126	101	129	117	123	133	40	34	36	25	32	32	34
105	111	101	100	113	93	106	131	104	117	128	124	148	41	35	40	39	47	36	35
107	103	104	104	120	101	121	116	135	111	108	121	109	42	37	41	42	29	31	29
110	127	104	119	135	103	127	143	126	123	137	125	120	42	41	34	23	31	27	30
98	119	90	99	129	99	112	127	126	127	116	109	99	36	38	48	33	26	37	32
92	92	84	109	115	100	117	90	121	124	106	108	86	37	31	35	36	33	38	36
107	106	109	112	143	105	109	127	128	139	118	125	71	35	33	39	27	31	40	39
105	93	120	113	109	89	115	137	116	96	106	96	76	48	36	28	32	33	33	29
106	117	103	127	107	121	104	113	137	125	101	106	66	39	35	30	31	47	38	32
115	99	121	117	112	107	109	131	101	119	107	103	67	44	36	26	32	36	31	32
111	132	85	122	110	97	120	110	123	124	93	110	71	26	31	26	33	41	39	27
119	101	121	90	100	97	114	128	96	102	109	79	47★	19	30	41	34	32	40	33
113	111	103	107	123	90	104	127	127	89	89	84	35	30	47	36	38	33	34	32
116	85	106	104	103	100	106	99	119	104	94	104	54	33	35	29	47	18	39	27
110	84	97	119	127	107	107	110	110	106	98	106	38	41	42	41	37	39	42	27
85	80	107	102	96	113	119	98	109	90	116	117	42	27	37	29	41	31	36	37
84	89	127	135	126	90	122	114	108	118	101	149	35	51	46	32	45	46	44	44
113	91	112	113	108	100	126	115	129	95	109	139	30	47	36	39	33	39	28	35
113	87	111	112	119	96	134	108	106	110	117	156	44	36	34	32	23	28	31	21
99	97	128	91	127	107	127	131	116	121	118	133	43	23	37	41	31	35	22	38

FIGURE 4.9.-- PHOTON COUNT vs TIME

H. BD +23° 536 (B color)

$m_v = 6.19$  AOV, B.C. = -0.17,  $T_e = 9600^\circ$

Computed blackbody diameter = 0".00019

Restoration limits:  $R_N = .00090$ ,  $R_A = .00029$ ,  $R_L = .00195$ ,  $R_T = 0.00033$

$S/N_0 = 4.4$

TABLE 4.11a

Restoration Data

$b_r$	$b_l$	$S/N_r$	F	$\Delta b_l$	$A_l$	$\Delta A_l$	$w_l$
.007565	.0123497	8.5	172	.0011790	9.389-5	2.913-5	0.118+10
.005752	.0120695	7.0	184	.0013220	1.108-4	3.191-5	0.098+10
.003782	.0121304	6.5	194	.0016380	1.301-4	3.976-5	0.063+10
A = 1.081-4, D = 3.252-5, X = 3.322							
diameter = 0".01040 $\pm$ 0".00171							

Figure 4.11 shows the unusual strip-brightness distribution curves derived from the restoration of this occultation curve. The restored diameter is over fifty times the computed blackbody diameter. The first maximum of the observed curve is 30% above the preoccultation intensity, as compared with only about 10% for a model occultation curve of diameter 0".010 (Figure A.2), and it is more typical of a star of diameter 0".004 in that respect.

The lunar limb velocity computed from the position of the first maximum is  $v_r = -.1640$  "/second. A lunar slope of about  $-22^\circ$  will account for the change from the predicted value of  $-.3213$  "/second. One Lunar Orbiter IV photograph, frame 193 1-of-3 high resolution, covers the region on the lunar surface which was the limb region for this occultation (selenographic coordinates  $\sim 52^\circ S$  and  $\sim 92^\circ W$ ). The lay of the land is not ruggedly mountainous but is obviously quite disturbed. The resolution of the orbiter photograph (80 m.)

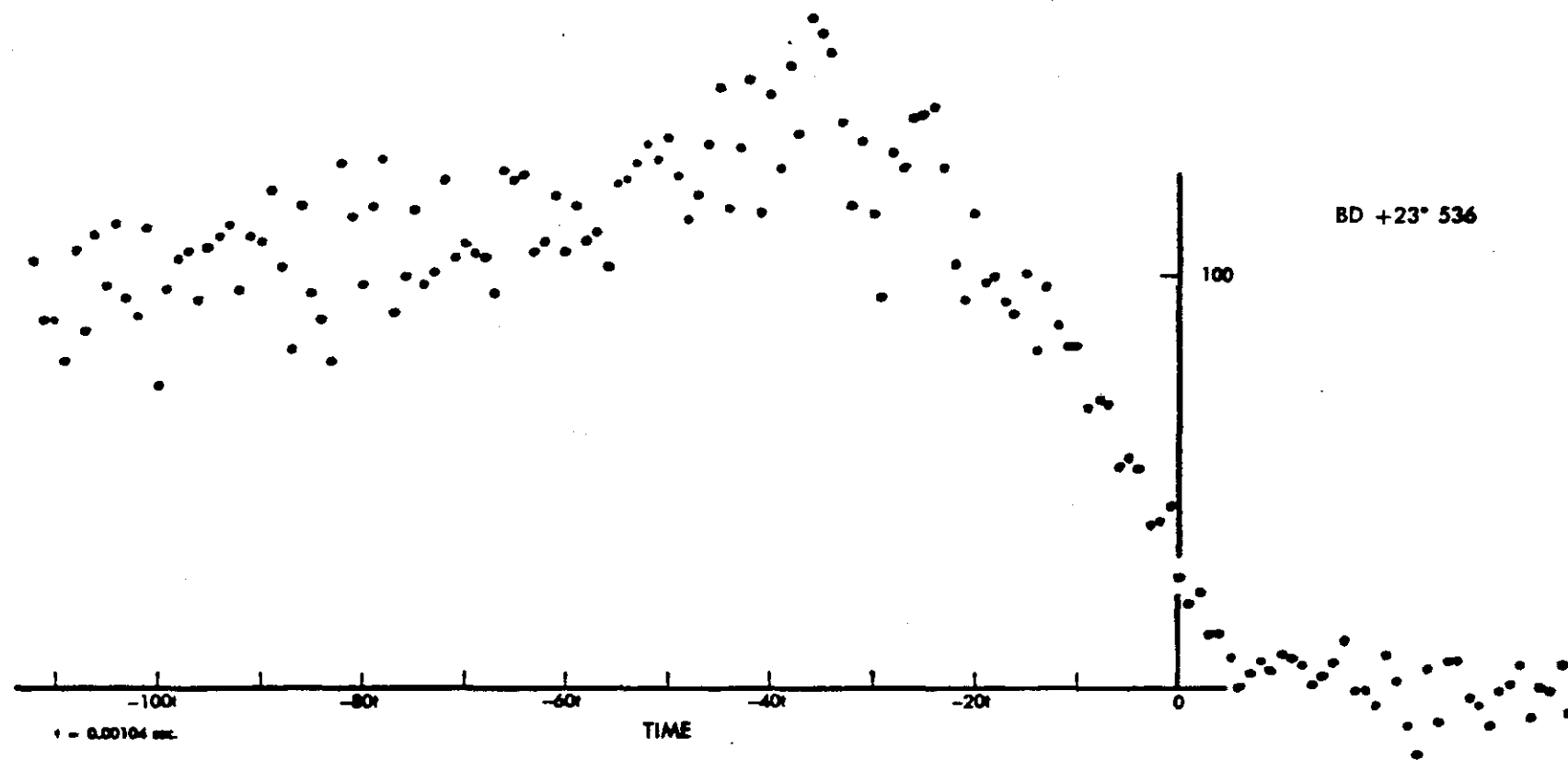
is not great enough to look for surface undulations or rocks on a scale of a few meters over which the occultation occurs. The sun angle is very low, however, and the shadows cast in a direction perpendicular to the "limb" also reveal a disturbed terrain.

The triplicity indicated by the restoration is probably not real in view of the effect the lunar limb plays on the occultation. Replacing the predicted limb velocity with the observed limb velocity reduces the computed angular diameter to  $0''.00567 \pm 0''.00092$  (Table 4.11b) and (not illustrated) eliminates the noise wiggles at the top of the restored curves. This occultation is quite noisy and plagued with limb irregularity; until more occultation observations are obtained little more should be said.

TABLE 4.11b

$b_r$	$b_l$	$S/N_r$	F	$\Delta b_l$	$A_l$	$\Delta A_l$	$w_l$
"005752	"0078180		180	"0006119	2.776-5	9.568-6	1.092+10
.003782	.0066231		181	.0006393	2.915-5	8.468-6	1.394+10
.002876	.0065853		201	.0007290	3.456-5	9.601-6	1.085+10
.002269	.0068431		228	.0008527	4.095-5	1.167-5	0.734+10

$A = 3.215-5,$        $D = 9.579-6,$        $X = 3.356$   
 diameter =  $0''00567 \pm 0''00092$



167	184	179	170	164	175	125	152	145	174	183	167	136	47	37	37	37	55	52	36
164	178	160	177	143	169	124	137	159	153	179	184	130	44	35	38	47	50	40	42
153	179	151	151	147	144	135	137	157	157	185	165	130	49	30	30	49	49	31	49
164	171	153	168	180	155	167	126	171	155	175	143	114	48	39	41	39	44	41	39
180	167	191	132	156	146	137	155	151	154	163	181	116	46	41	45	40	47	37	38
173	157	159	166	154	159	171	134	129	144	170	177	115	41	46	43	45	47	43	46
165	182	143	142	158	155	134	159	167	176	183	190	99	43	32	48	37	38	47	40
166	141	143	125	160	175	128	146	144	174	198	191	101	47	40	44	49	42	39	39
167	183	143	175	168	143	158	162	137	175	166	193	98	53	39	47	38	39	38	53
164	166	157	175	177	151	142	143	126	155	182	177	83	39	46	49	41	52	38	35
183	176	151	159	177	161	137	138	178	158	200	152	84	39	33	38	50	35	37	45
152	167	131	165	155	143	120	161	164	170	165	142	88	35	40	59	33	32	32	34
178	143	138	163	166	154	151	120	146	155	196	165	69★	49	34	43	48	33	35	41
164	183	149	163	150	155	127	145	167	167	177	147	62	42	42	37	40	51	45	32
179	178	159	161	148	156	128	153	179	158	204	148	65	30	41	40	31	33	39	34
180	171	165	161	167	154	132	155	139	160	186	142	54	22	43	44	47	31	42	40
195	159	130	173	143	151	135	142	148	151	216	139	54	45	44	35	36	34	41	42
176	167	144	187	169	166	136	156	166	173	212	149	48	31	31	40	31	42	46	41
179	167	169	170	172	139	142	159	146	174	207	129	41	47	54	39	38	43	44	36
156	183	168	166	159	135	133	162	149	178	189	146	44	47	32	37	52	37	40	34

FIGURE 4.10.-- PHOTON COUNT vs TIME

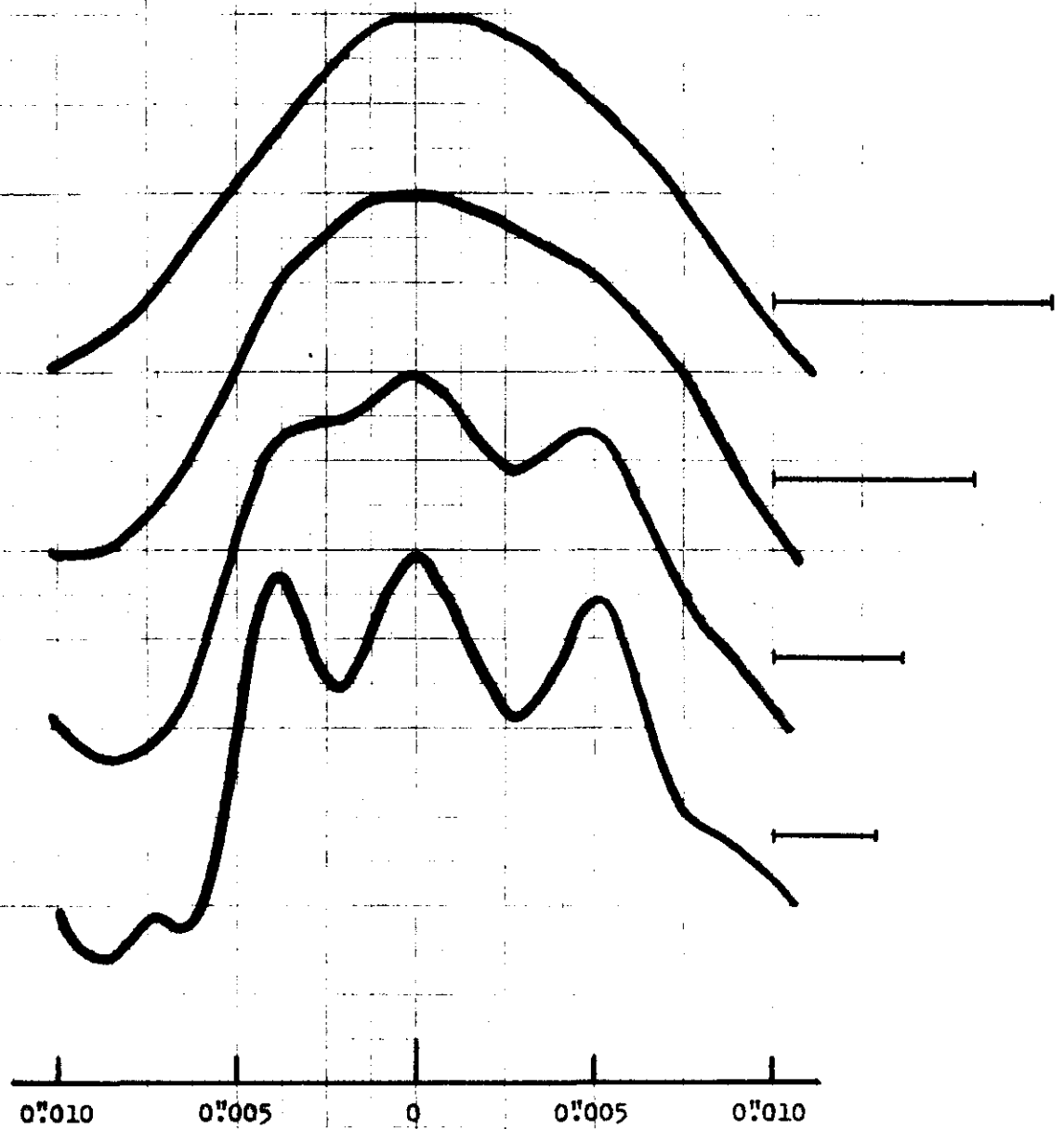


Fig. 4.11.--Restoration Curves for BD +23° 536

## I. BD +23° 541 (b color)

$m_v = 2.77$  B7III, B.C. = -0.91,  $T_e = 13600^\circ$

Computed blackbody diameter = 0".00063

Restoration limits:  $R_N = .00115$ ,  $R_A = .00029$ ,  $R_L = .00084$ ,  $R_T = .00030$

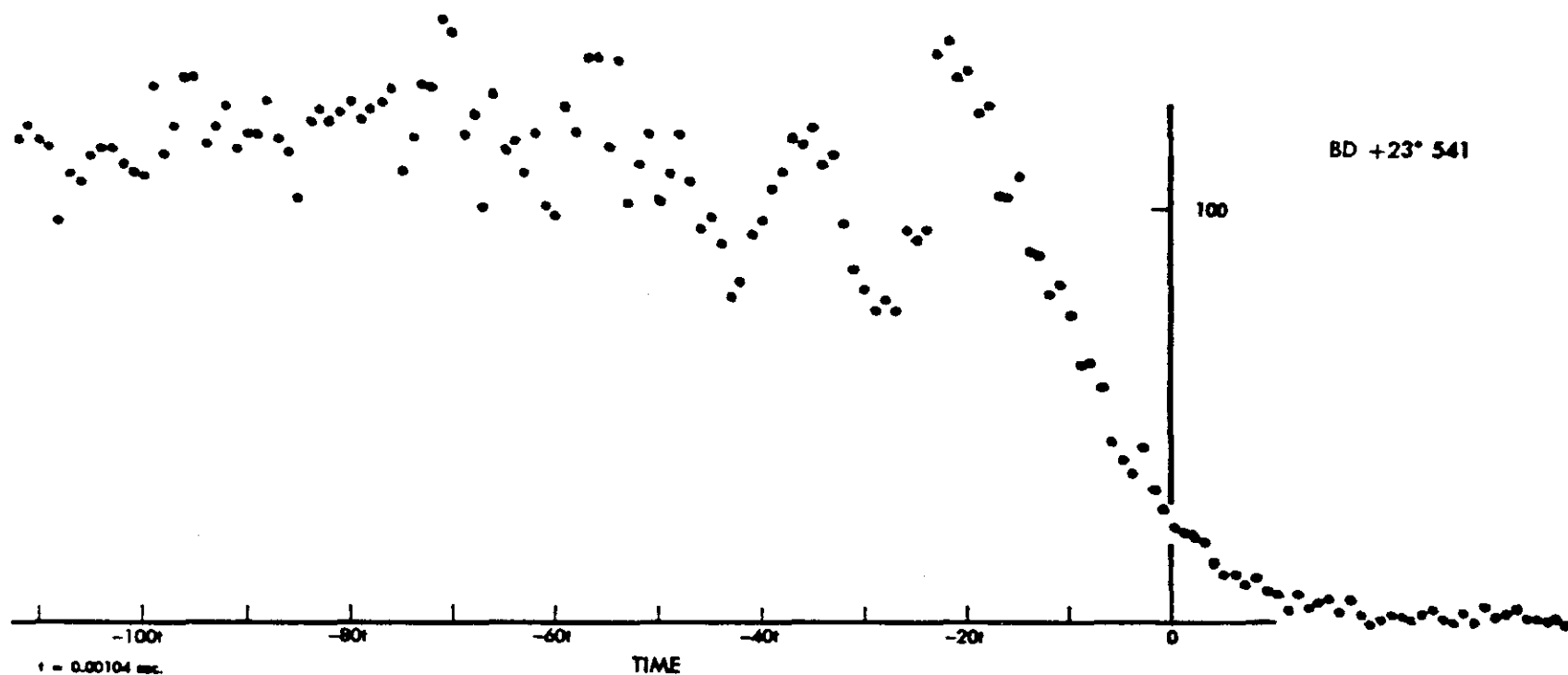
$S/N_0 = 3.7$

TABLE 4.12

## Restoration Data

$b_r$	$b_l$	$S/N_r$	F	$\Delta b_l$	$A_l$	$\Delta A_l$	$w_l$
.017716	.0207459		243	.0014670	1.147-4	6.091-5	0.027+10
.007766	.0076912		174	.0008214	1.830-6	1.263-5	0.626+10
.005905	.0060730		179	.0007438	1.459-6	9.034-6	1.255+10
.003883	.0042274	9.0	183	.0006384	2.385-6	5.398-6	3.431+10
.002953	.0029155	7.5	172	.0005049	-4.750-7	2.944-6	11.53+10
.002330	.0022821	6.0	165	.0004449	-4.189-7	2.030-6	24.24+10
.001772	.0020009	4.5	175	.0004473	6.634-7	1.790-6	31.20+10
A = 2.349-7, D = 2.465-6, X = .095							
diameter = 0".00164							

This star was included in the radial velocity study of the Pleiades by Abt, et. al. (op. cit.). Their observations did not confirm an earlier suspicion of variability (Smith and Struve 1944). Although quite noisy, the occultation curve does not reveal a secondary component at scan position angle 135°. The upper limit derived here for the angular diameter is only slightly above the computed blackbody diameter. This occultation occurred at about the same selenographic position as the occultation of BD+23° 536, but unlike that occultation the lunar slope for this disappearance is nominally zero--the observed fringe maxima occur in time exactly where they are predicted to occur.



272	307	271	343	271	305	255	248	255	255	234	165	139	12	9	2	7	4	2	4
278	299	241	325	286	311	241	210	271	265	254	171	139	20	10	7	4	6	5	5
267	286	267	308	275	251	227	234	251	217	231	162	126	14	13	6	9	6	7	6
266	266	253	357	284	260	215	230	245	275	207	206	99	16	9	6	7	3	9	2
267	285	274	324	269	259	187	243	222	247	212	201	88	18	7	7	9	11	2	10
295	324	271	341	265	207	223	247	261	251	159	206	82	12	5	7	7	1	7	2
262	297	319	370	279	253	214	247	266	235	177	295	95	17	7	5	7	5	4	4
300	315	307	334	305	244	203	239	262	255	179	301	74	10	5	4	3	6	7	3
286	315	232	275	271	215	200	235	265	217	204	283	64	4	6	7	5	4	5	10
291	304	316	324	307	232	207	232	271	213	211	286	55★	6	10	8	7	11	5	9
306	312	248	325	302	213	227	271	262	268	227	265	52	9	5	5	5	5	4	7
266	312	267	291	288	223	214	245	267	256	235	268	50	9	6	5	3	3	4	8
316	351	311	267	330	200	230	284	171	262	251	223	47	7	9	1	4	2	3	5
269	314	329	276	314	192	235	288	271	253	249	223	36	9	3	5	10	5	3	6
275	316	305	266	315	227	215	237	239	248	257	232	31	12	6	5	3	2	8	2
311	303	309	274	322	210	231	257	251	251	235	195	31	8	5	9	5	3	4	4
302	303	324	277	315	193	245	267	257	215	242	192	26	5	4	4	3	7	9	11
301	320	235	243	260	213	203	268	278	229	209	173	29	10	6	3	3	2	9	6
292	321	407	255	321	202	254	247	312	254	184	174	22	5	7	5	5	2	5	7
327	289	331	249	229	222	251	255	305	221	175	163	20	14	5	4	5	8	7	3

FIGURE 4.12.-- PHOTON COUNT vs TIME



J. BD +23° 541 (y color)

$m_V = 2.77$  B7III, B.C. = -0.91,  $T_e = 13600^\circ$

Computed blackbody diameter = 0".00063

Restoration limits:  $R_N = .00136$ ,  $R_A = .00029$ ,  $R_L = .00095$ ,  $R_T = .00030$

$S/N_o = 3.4$

TABLE 4.13

Restoration Data

$b_r$	$b_l$	$S/N_r$	F	$\Delta b_l$	$A_l$	$\Delta A_l$	$w_l$
.004191	.0041275	17.	154	.0006530	-9.546-7	5.390-6	3.441+10
.003186	.0032095	12.	157	.0005823	-1.888-7	3.738-6	7.155+10
.002514	.0027342	10.	162	.0005585	8.437-7	3.054-6	10.72+10
.001912	.0025604	6.5	183	.0005997	2.540-6	3.071-6	10.60+10
.001676	.0025596	5.5	197	.0006403	3.332-6	3.278-6	9.305+10
$A = 1.512-6, \quad D = 3.423-6, \quad X = .441$ diameter = 0".00222							

Combining this observation with its companion b-color observation, the weighted upper limit to the diameter is 0".00188. No evidence for either stellar or lunar irregularities exists in the observations.

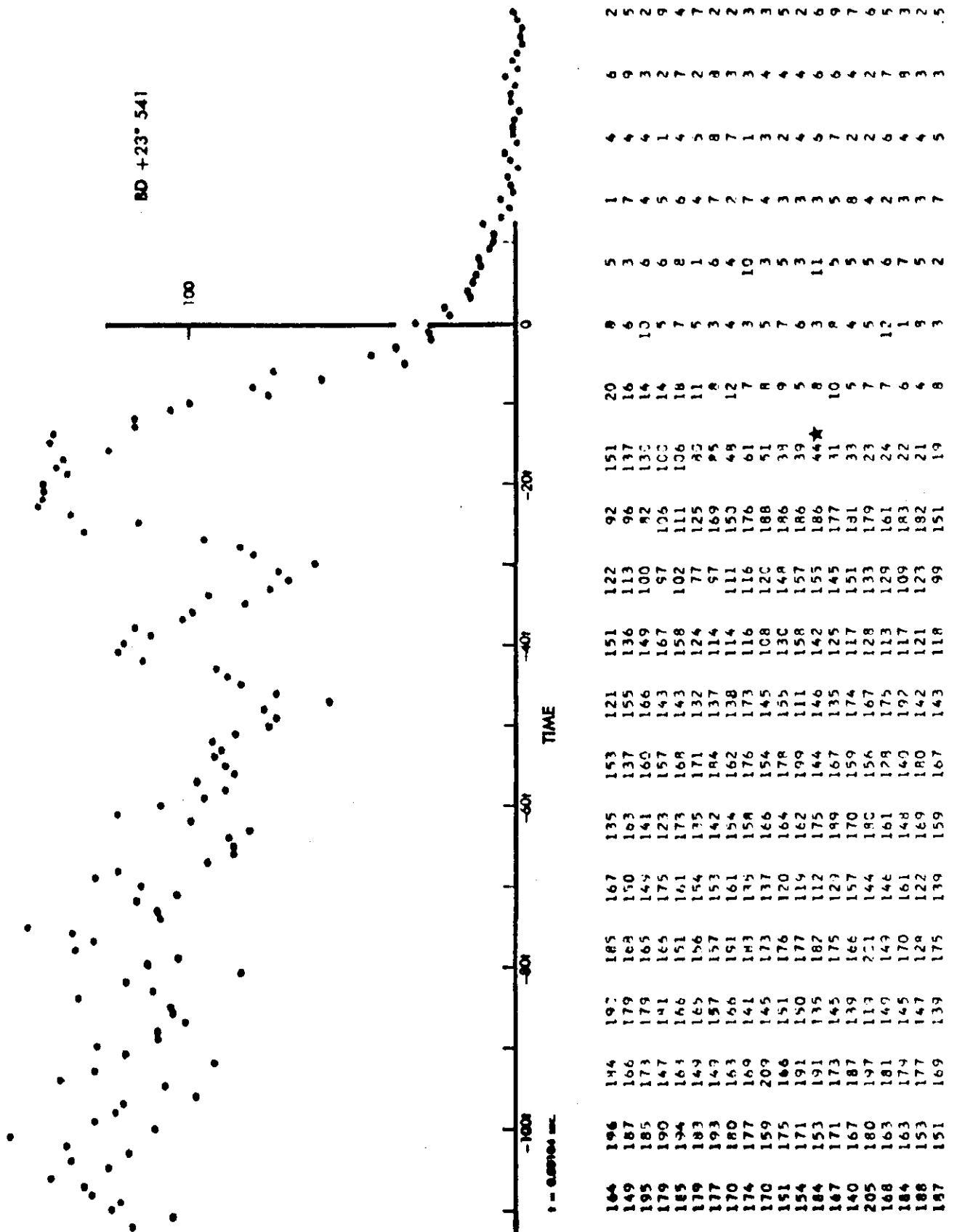


FIGURE 4.13.-- PHOTON COUNT VS TIME

### K. Other Observations.

In addition to the occultations of seven stars reported here in detail, 58 occultations were observed in the course of fifteen months between December 1967 and March 1969. While these data are of little or no value for analytical interpretation, they serve to establish empirical limits to the observational technique.

Table 4.14, for instance, lists 36 occultations which were not recovered from the data tape because the occultation could not be found when the tape was replayed on an oscilloscope. The table gives the names, magnitudes, spectral types, and filter used. For three of them, marked with an asterisk, a tape recorder failure at the time of observation left only blank tape in place of recorded data. Table 4.15, in the same format as Table 4.14, lists 22 occultations which were recovered from the data tape but which were not reduced because of low signal/noise. Although some of the stars are intrinsically very bright, atmospheric extinction frequently had eliminated any advantages of increased stellar brightness. Recovery and analysis of the data is also a function of the phase of the moon. For this reason BD-13°6257 (43% illumination) was recovered while BD+10° 242, approximately equal in magnitude and spectral type (81% illumination), could not be recovered.

From these tables the following conclusions are drawn: a) observations of stars of visual magnitude 9.0 and fainter are worthless--the probability of determining diameters, discovering duplicity, or even recovering the data is for practical purposes zero; b) stars of 8<sup>th</sup> magnitude can probably be recovered but are probably of little astrophysical value; and c) for 6<sup>th</sup> and 7<sup>th</sup> magnitude stars observations can be either good or bad, depending on lunar illumination and atmospheric extinction. These conclusions apply, of course, only to observations with a 32-inch to 36-inch telescope.

TABLE 4.14

Occultations of Stars That Could Not Be  
Recovered from the Data Tape

NAME	MAG	SP	FILTER
CD -23° 16668	8.7	G0	V
CD -23° 16668	8.7	G0	B
CD -23° 16675	9.3	K	v
CD -22° 15116	9.0	F5	v
CD -22° 15178	9.4	F5	B
CD -22° 15182	8.8	K0	y
CD -22° 15187	9.6	G5	B
CD -22° 15195	9.5	F8	B
CD -22° 15197	9.2	F8	B
BD -18° 6042	9.0	K0	B
BD -12° 6351	9.3	K5	B
BD - 7° 6037	9.1	A0	B
BD - 1° 13	9.4	G5	B
BD - 1° 15	8.3	K0	V
BD - 1° 15	8.3	K0	B
BD + 3° 127	8.7	K2	B
BD + 3° 132	9.0	F8	B
BD + 4° 145	9.1	G0	v
BD + 4° 150	9.1	A0	v
BD + 4° 156	8.8	G0	B
BD + 4° 157	8.6	K2	v
BD + 5° 140	8.7	G0	B
BD + 9° 199	8.4	G0	v
BD + 9° 203	8.4	F8	v
BD + 9° 204	9.2	F8	v
BD +10° 234	8.7	K5	v
BD +10° 235	8.8	A5	v
BD +10° 237	8.6	F8	v
BD +10° 242	8.6	K2	v
BD +23° 503	8.8	A2	B
BD +23° 519	8.2	K2	B
BD +23° 549	8.3	A3	B
BD +23° 554	8.6	F8	B
BD +23° 558	5.1	B8p	B*
BD +23° 561	6.6	B9	B*
BD +23° 567	7.3	A0	B*

TABLE 4.15

Occultations of Stars That Were Recovered  
But Not Analyzed

NAME	MAG	SP	FILTER
BD -18° 6052	7.8	A5	B
BD -17° 6412	8.8	G0	B
BD -16° 6046	6.6	G5	b
BD -13° 6257	8.6	K0	B
BD -12° 6340	8.3	K0	B
BD -12° 6350	8.5	F0	B
BD + 4° 159	8.3	A5	B
BD + 4° 172	6.2	K2	y
BD + 4° 172	6.2	K2	b
BD + 6° 2437	4.1	B9V	v
BD + 9° 194	8.3	F5	v
BD + 9° 206	8.4	A2	v
BD +23° 495	8.3	A5	B
BD +23° 510	8.1	A3	B
BD +23° 512	8.2	B9	b
BD +23° 516	3.9	B7	b
BD +23° 516	3.9	B7	y
BD +23° 517	8.0	A0	B
BD +23° 523	7.0	A0	B
BD +23° 553	6.6	A0	B
BD +23° 558	5.1	B8p	B
BD +23° 562	6.7	B9	B

## V. Remarks

### A. Lunar Slopes.

The occultation of BD +24° 547 provides an excellent opportunity to make an independent determination of the lunar slope at the point of disappearance. Such determinations are always possible from occultations, but the accuracy is considerably enhanced for graze or near-graze circumstances. Such is the case for this occultation.

There is an error in a prediction parameter-- $v_r$ ,  $b$ ,  $\lambda$ , or  $t_o$ --for this occultation. This fact is deduced by normalizing the observed curves (both colors, Figures 4.7 and 4.8) to unitless parameter  $w$  in the abscissa and unit intensity in height. Observations so normalized are observations in the "w-I" plane. A comparison in the w-I plane of these curves with a pointsource model shows that the fringes are not superimposed horizontally.

The error does not occur in  $t_o$ , the time of occultation, since a lateral shift of the zero point of the curve is not adequate for superposition of the fringes. Successive fringes are increasingly out of phase; therefore a change of scale needs to be made. The error is not in the wavelength parameter,  $\lambda$ . The V-color curve superimposes almost exactly on the B-color curve when both are reduced to the w-I plane. Furthermore, observations of other occultations in these colors do not indicate errors in wavelength, as they are correctly superimposed on model curves in the w-I plane. The distance to the limb,  $b$ , is not in error since a correction of  $0.48 \times 10^8$  m. would be required to produce the necessary fringe expansion, placing the moon at a distance of  $4.44 \times 10^8$  meters, or 16% above the mean distance. The maximum variation in the distance of the moon above the mean is on the order of 7%. A change in the velocity of the lunar limb,  $v_r$ , however, is of the order of magnitude necessary to produce the observed fringe phase effect. A logical

cause, namely a lunar slope, can be invoked to account for the change in velocity.

Equation (2.5) gives the relation between  $t$ ,  $v_r$ ,  $b$ ,  $\lambda$ , and  $w$ , viz.,

$$w = 4.8481 \times 10^{-6} v_r t \sqrt{\frac{2b}{\lambda}}.$$

Inverting and solving for  $v_r$ , this equation becomes

$$v_r = 206264.8 \frac{w}{t} \sqrt{\frac{\lambda}{2b}}. \quad (5.1)$$

A value of  $v_r$  computed from observed values of  $t$ ,  $w$ ,  $\lambda$ , and  $b$  is compared with the predicted value of  $v_r$ , the difference is attributed to a lunar slope, and the lunar slope is found.

For the B-color observation of BD +24° 547,  $\lambda = 4.44 \times 10^{-7}$  meters,  $b = 3.967 \times 10^8$  meters, and the first and second maxima occur in channels -26 and -50, respectively, or  $t_1 = -26 \times .00104 = -.02704$  seconds, and  $t_3 = -.05200$  seconds. The first minimum occurs in channel -40, or  $t_2 = -.04160$  sec. Because the observations are reduced to the  $w$ -I plane, the first and second maxima and first minimum are required to fall at  $w = 1.225$ ,  $2.345$ , and  $1.871$ , respectively. The average time is  $\bar{t} = -.040213$ , and the average  $\star$  is  $1.8137$ . Using equation (5.1)  $v_r$  is found to be

$$v_{r,c} = -.2202 \text{ "/second}. \quad (5.2a)$$

For the V-color observation  $\lambda = 5.47 \times 10^{-7}$  meters,  $t_1 = \text{ch } -29 = -.03016$  seconds,  $t_2 = \text{ch } -44 = -.04576$  seconds, and  $t_3 = \text{ch } -55 = -.05720$  seconds. For this observation the average  $t = -.044373$ , and  $v_r$  is found to be

$$v_{r,c} = -.2213 \text{ "/second}, \quad (5.2b)$$

which agrees nicely with (5.2a). An average value  $v_{r,c} = -.2207 \text{ "/second}$  will be taken as the correct lunar limb velocity.

The slope of the lunar surface can be found when the angle between the velocity vector of the moon and the radius vector to the star at disappearance is known. Occultation predictions give this angle. In Figure 5.1 let  $\zeta$  be that angle. If  $\xi$  is the angle between the surface normal and the velocity vector at the point of disappearance, then the difference,  $\zeta - \xi$ , will give the lunar slope. Letting  $v_p$  = the predicted velocity of the lunar limb along

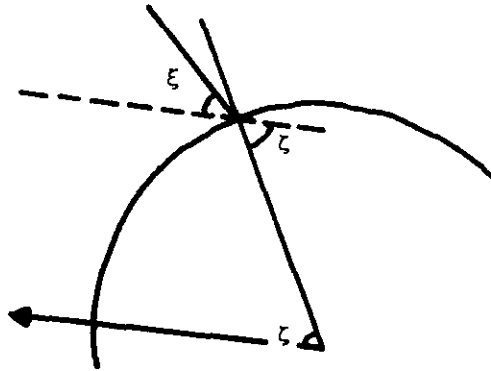


Fig. 5.1.--Occultation Geometry

the radius vector to the star at disappearance and  $v_t$  = the observed, true lunar limb velocity, the slope is found by

$$\text{slope} = \zeta - \xi = \zeta - \cos^{-1}\{v_t \cos \zeta / v_p\}. \quad (5.3)$$

Using the values  $v_p = -.1930$  "/second,  $v_t = -.2207$  "/second, and  $\zeta = 63^\circ 9$ , the slope is computed to be  $4^\circ 1 \pm 0^\circ 1$ .

From Watts' (1963) Marginal Zone Catalog data, the approximate profile of the lunar limb at the occultation point can be plotted. The axis angles and elevations read from the charts at the appropriate values of librations are given in Table 5.1. They are plotted in Figure 5.2, where the vertical scale is expanded with respect to the horizontal scale for clarity.



TABLE 5.1

Axis Angles and Elevations  
at LIBA 2.10, LIBB -5.67

AXIS ANGLE	HORIZONTAL POSITION	ELEV.
29°6	0"0	-1"05
29.8	3.255	-1.05
30.0	6.510	-0.92
30.2	9.765	-0.80
30.4	13.020	-0.85
30.6	16.275	-0.80

The axis angle (abscissa) is tabulated in both seconds of arc and degrees, and the elevations are in seconds of arc. Using a simple rise-over-run

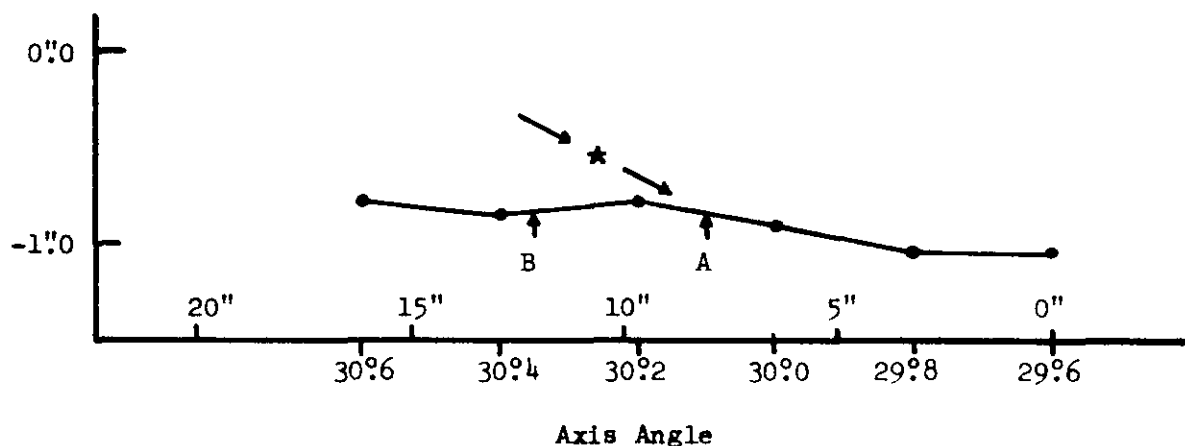


Fig. 5.2.--Lunar Profile for the Occultation of BD +24° 547

calculation for the slope at the predicted axis angle of 30°1 (point A in Figure 5.2), the slope is  $\tan^{-1}[.12/3.255] = 2^\circ.1$ . This does not agree with the value  $4^\circ.1$  computed above. Moreover the slope is in the wrong direction, effectively decreasing the lunar limb velocity. However, van Flandern (1965) and Dunham (1969) indicate that, based on grazing occultations, a systematic correction of +0°2 to +0°3 should be applied to the predicted axis angle. This has the effect of moving the point of disappearance from point A to

point B in Figure 5.2 (axis angle  $30^{\circ}35'$ ). The slope at point B is  $\tan^{-1}[.05/3.255] = 0^{\circ}9'$ , agreeing only in direction with the slope computed from the occultation curve.

Figure 5.3 is a contour diagram of equation (5.3) in which the lunar slope is plotted as a function of the parameter  $R$ , where  $R = v_t/v_p$ , and  $\zeta$ , the angle between the lunar velocity vector and the radius vector to the point of disappearance. The curve has variable horizontal scales in three sections as indicated. Negative slopes slow down the fringes, and positive slopes speed up the fringes, except in the region between  $\zeta = 0^{\circ}$  and  $\zeta = 10^{\circ}$ , for  $R < 1$ , where ambiguities are possible. When one determines a true lunar limb speed from observation, the lunar surface slope can be found by entering Figure 5.3 with the appropriate values of  $R$  and  $\zeta$ .

#### B. Angular Separation, Parallax, and Orbital Inclination.

The measurement of angular separations and position angles of binary star components from lunar occultations belongs to the realm of "visual" binary observations except that separations can be found which are an order of magnitude or more smaller than minimum visual separations. A single occultation observation by a lone observer provides only the separation of components at the scan position angle. Two or more "simultaneous" observations from different sites are required to solve for true position angle and separation unambiguously.

In the apparent orbit of a binary system the position of the secondary component is derived from the projection equations (Binnendijk 1960) to be

$$\begin{aligned} \rho \cos(\theta - \Omega) &= r \cos(u + \omega) \\ \rho \sin(\theta - \Omega) &= r \sin(u + \omega) \cos i \end{aligned} \quad (5.4)$$

where the angles have the usual meanings. Squaring and adding each term of equation (5.4) gives

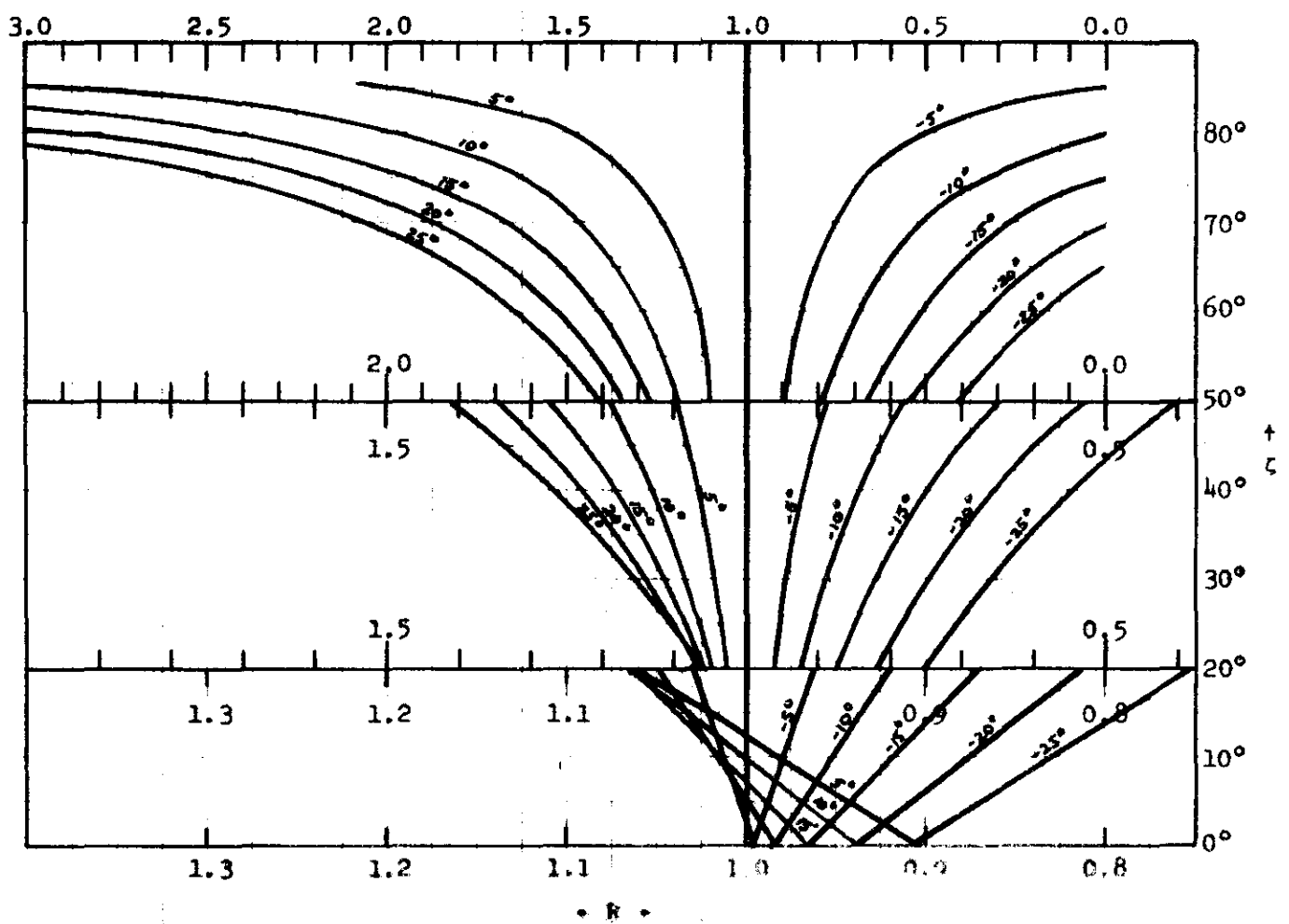


Fig. 5.3.--Lunar Slopes,  $t, s + 1.2$ .

$$\rho^2 = r^2 (1 - \sin^2(u + \omega) \sin^2 i) \quad (5.5)$$

The substitution of  $r = a(1 - e \cos E)$  is made:

$$\rho = a(1 - e \cos E) \sqrt{1 - \sin^2(u + \omega) \sin^2 i}. \quad (5.6)$$

Multiplying the right side by  $\sin i / \sin i$  and converting to seconds of arc gives

$$\rho'' = \frac{\pi''}{k} (a \sin i) \{1 - e \cos E\} \sqrt{\frac{1 - \sin^2(u + \omega) \sin^2 i}{\sin^2 i}} \quad (5.7)$$

where  $\pi''$  is the parallax of the star in seconds of arc and  $k = 149,5985 \times 10^6$  km.

If the spectroscopic elements of the binary system,  $e$ ,  $\omega$ ,  $a \sin i$ ,  $T$ , and  $P$ , are known independently,  $E$  and  $u$  are found for the time of observation, and equation (5.7) relates the parallax, inclination, and angular separation.

In this representation the longitude of the node,  $\Omega$ , which is unknown from spectroscopic studies, drops out. The angular separation is dependent to a large extent on the value of  $i$ , so that a single separation measurement, combined with a known parallax, will provide a determination of the orbital inclination. For the three stars in this study with known spectroscopic elements, Table 5.2 lists the computed values of phase,  $Ph$ , in cycles since the epoch, the eccentric anomaly,  $E$ , and true anomaly,  $u$ , in degrees, and the angular separation,  $\rho$ , in seconds of arc. A distance of 126 parsecs is assumed.

TABLE 5.2

Orbital Data of Spectroscopic Binaries

NAME	Ph	E	u	$\rho$
BD+23° 507	157.582	199°5	191°0	$.00243/\{1 - .0365\sin^2 i\}/\sin^2 i$
BD+23° 540	15114.682	244.6	243.6	$.00043/\{1 - .0226\sin^2 i\}/\sin^2 i$
BD+24° 547	12.974	350.0	349.2	$.00709/\{1 - .9997\sin^2 i\}/\sin^2 i$

## C. Photon Counter Capability.

Two empirical tests of photometer counting accuracy were made. For the first test, at Kitt Peak National Observatory on 7 December 1967 UT, four stars were observed in the single-channel mode with the photomultipliers biased at 1200v DC. The observations were made away from the moon in relatively dark, clear and calm skies. Table 5.3 lists the stars, their magnitudes and spectral types from the Arizona-Tonanzintla Catalog (Sky and Telescope, 30, 24, 1965), and the observed counts per 1.04 milliseconds averaged over about one-eighth second. Three filters were used--y, v, and B. The sequence of observations, 163y-v-B, 154y-v-B, 165y-v-B, and 39y-v-B, was accomplished in less than 10 minutes. The first line under COUNTS indicates the average counts per integration cycle, the second line is the one sigma error, and the third line is the expected square-root dispersion. Figure 5.4 shows graphi-

TABLE 5.3

## Observations of Standard Stars at Kitt Peak

NAME	$m_v$	$m_B$	Sp	COUNTS		
				y	v	B
39 $\gamma$ Peg	2.86	2.65	B2IV	880.2	1527.1	overload
				26.2	24.8	
				29.7	39.1	
154 $\pi$ And	4.36	4.20	B5V	252.5	491.8	1880
				15.7	23.4	27.4
				15.9	22.2	43.3
163 $\epsilon$ And	4.39	5.26	G8IIIp	258.9	138.2	1225
				16.0	9.9	31.8
				16.1	11.7	35.0
165 $\delta$ And	3.30	4.60	K3III	647.9	194.0	1728
				25.4	13.6	26.5
				25.5	13.9	41.5

cally the observed counts (ordinate) versus the one-sigma observed dispersion (abscissa). The dashed curve is the theoretical square-root dispersion.

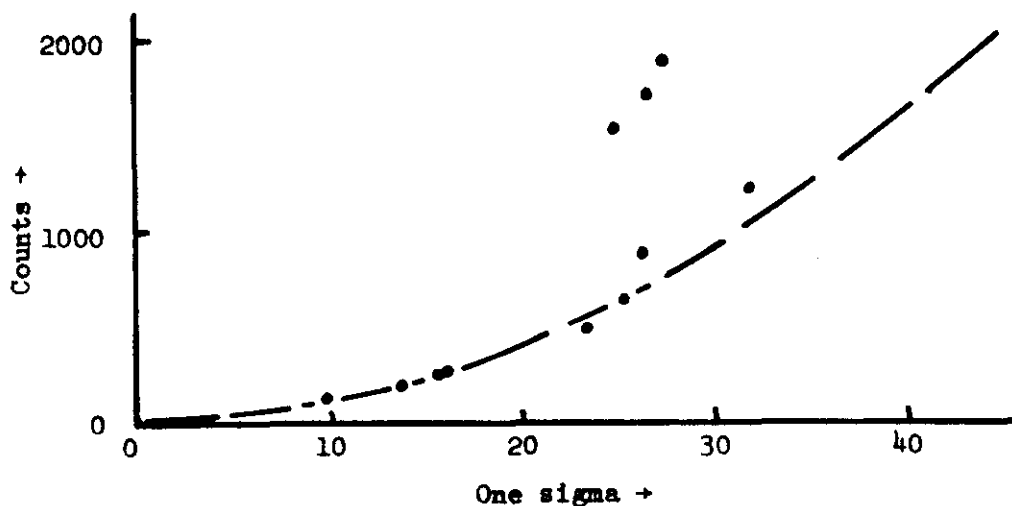


Fig. 5.4.--Counts vs. One-sigma Dispersion

For the second test, a Datatech pulse generator was used to simulate a photomultiplier by generating equally spaced rectangular pulses of thirty nanoseconds width, variable frequency, and sufficient negative gain to trigger the input counter gate. These pulses were fed to the counter through the preamplifier and amplifier. Input rates, as measured by a General Radio digital frequency meter, were compared to output rates as measured by the binary counter. The counter operated linearly up to 8 Mhz at which point the GR meter failed, and continued to count to a frequency of about 12.5 Mhz. The binary counter stopped when the pulses were 80 nanoseconds apart.

Three conclusions are drawn from these tests. First, the counter operates linearly up to high rates when input pulses are sufficiently narrow and well-shaped. Second, the failure of observed counts to follow a square-root dispersion at high rates is a result of pulse coincidence, indicating that photomultiplier pulses after preamplification and amplification are neither sufficiently narrow nor well-shaped. Finally, for the observations discussed in this paper, pulse coincidence can be ignored since the observed rates do

not exceed 500 khz. Enhancement of the pulse counter accuracy can be achieved through improvement of the preamplifier and amplifier circuits, which in their present configuration must degrade the input photoelectric pulses. This should be especially important for observations of bright stars, where the expected counts per integration cycle will be quite high.

#### D. Restorations of Model Occultations.

An empirical test of equation (2.22) was made by using equation (2.7) to generate model occultation curves with signal/noises = 250, 100, 10, and 6, for uniform brightness ( $\beta_\lambda = 0$ ) and various diameters up to 0".010. When the S/N was high the limit for the restoration beamwidth was most often equal to 0".001818 because of the limited extent of the generated model curves. In other cases, the limiting restoration beamwidth was that which produced a restored curve with signal/noise = 5. Table 5.4 gives the recovered diameters of test sources, the calculated mean error (%) = computed mean error  $\div$  recovered diameter, and the true errors (%) = (recovered diameter - true diameter)  $\div$  true diameter, as a function of signal/noise. When no calculated mean error is given, only an upper limit to the diameter was derived from the restoration.

One interesting conclusion gleaned from model studies is that for observations with very high signal/noise, equation (2.22) does not give correct diameters to within the mean error confidence interval! The recovered diameters are more than 30% too low.

One would first suspect the generated curves of being faulty. Occultation curves were regenerated for a few of the smaller sources using equation (2.6). In no case was there a significant difference noted in the occultation curves, especially in the higher-order fringes where a difference would more easily show up. A moment's reflection uncovers a number of reasons for the disparity found above.

First, the strip-brightness distribution for a uniform disc ( $\beta_\lambda = 0$ ) is

TABLE 5.4

## Recovered Diameters of Test Sources

True Diameters	Recovered Diameters	Calculated Mean Error (68.2% Conf)	True Error	
0.0005	0.000332±0.000075	±22.6%	-33.6%	S/N <sub>o</sub> = 250
0.001	0.000611 0.000036	5.9	-38.9	
0.002	0.001228 0.000021	1.7	-39.6	
0.003	0.001887 0.000018	1.0	-37.4	
0.004	0.002565 0.000018	0.7	-35.9	
0.005	0.003283 0.000019	0.6	-34.6	
0.006	0.004019 0.000021	0.5	-33.1	
0.008	0.005553 0.000024	0.4	-30.6	
0.01	0.006955 0.000026	0.4	-30.5	
0.0005	0.000458 0.000124	27.1	- 8.4	S/N <sub>o</sub> = 100
0.001	0.000686 0.000076	10.9	-31.4	
0.002	0.001283 0.000050	3.9	-35.8	
0.003	0.001978 0.000045	2.0	-34.1	
0.004	0.002702 0.000046	1.7	-32.4	
0.005	0.003470 0.000049	1.4	-30.6	
0.006	0.004229 0.000052	1.2	-29.4	
0.008	0.005739 0.000059	1.0	-28.4	
0.01	0.007295 0.000066	0.8	-27.1	
0.0005	0.000948 0.		+89.6	S/N <sub>o</sub> = 10
0.001	0.001404 0.		+140.	
0.002	0.000896 0.		-55.3	
0.003	0.001676 0.000793	47.3	-44.2	
0.004	0.001859 0.000885	47.6	-53.6	
0.005	0.002451 0.000564	22.1	-51.0	
0.006	0.002809 0.000546	19.4	-53.2	
0.008	0.005385 0.000677	12.6	-32.8	
0.0005	0.001158 0.		+131.	S/N <sub>o</sub> = 6
0.001	0.001115 0.		+11.2	
0.002	0.001123 0.		-48.4	
0.003	0.002314 0.		-22.8	
0.004	0.001959 0.		-51.0	
0.005	0.001688 0.001098	65.9	-66.2	
0.006	0.002084 0.001552	74.4	-65.3	
0.008	0.005382±0.001844	±34.3%	-32.7%	



$$B(x)dx = a\sqrt{1-x^2} \quad (5.8)$$

so that the angular diameter of the most well-resolved source of the highest signal/noise will approach only 86.6% of the true angular diameter,  $\phi$ , when measured at the half-intensity point. In other words, as  $b_r \rightarrow 0$ ,  $b_l \rightarrow .866\phi$ . Further, if the disc is completely darkened ( $\beta_\lambda = 1$ ) then

$$B(x)dx = a(1-x^2) \quad (5.9)$$

and  $b_l \rightarrow .707\phi$  as  $b_r \rightarrow 0$ . This accounts for at least 14% of the true error for a uniformly illuminated disc.

Second, the observed strip-brightness distribution, the restored curve, is not the convolution of a gaussian restoring beam with another gaussian source (from which von Hoerner's results are derived); rather it is the convolution of a gaussian with a  $\sqrt{1-x^2}$  function (see equation (2.13) with  $t(x) = \text{equation (A.3)}$ ). Figure 5.5 shows the curve  $f(x) = g(x)*t(x)$  for three gaussians,  $g(x)$ , with widths equal to  $0.1\phi$ ,  $0.25\phi$ , and  $\phi$ . For various restoration resolutions, the half-intensity width of the observed curve can be either greater than or less than the true diameter. This is never the case when two gaussians are convolved.

Without a more complete analytical analysis of this phenomenon it is difficult to judge the degree to which it has an effect on diameter determinations. It is conceivable that the remaining error is caused by just such a phenomenon. Another possible explanation for large true errors at high signal/noise could be the failure to restore down to the noise limit, which, for the model with  $S/N = 250$ , is  $3 \times 10^{-7}$  seconds of arc.

At the other end of the scale, for small sources with low signal/noise, it is seen that the noise limit has been reached, and stars have apparent angular diameter upper limits of the order of  $0''.001$ . This agrees well with

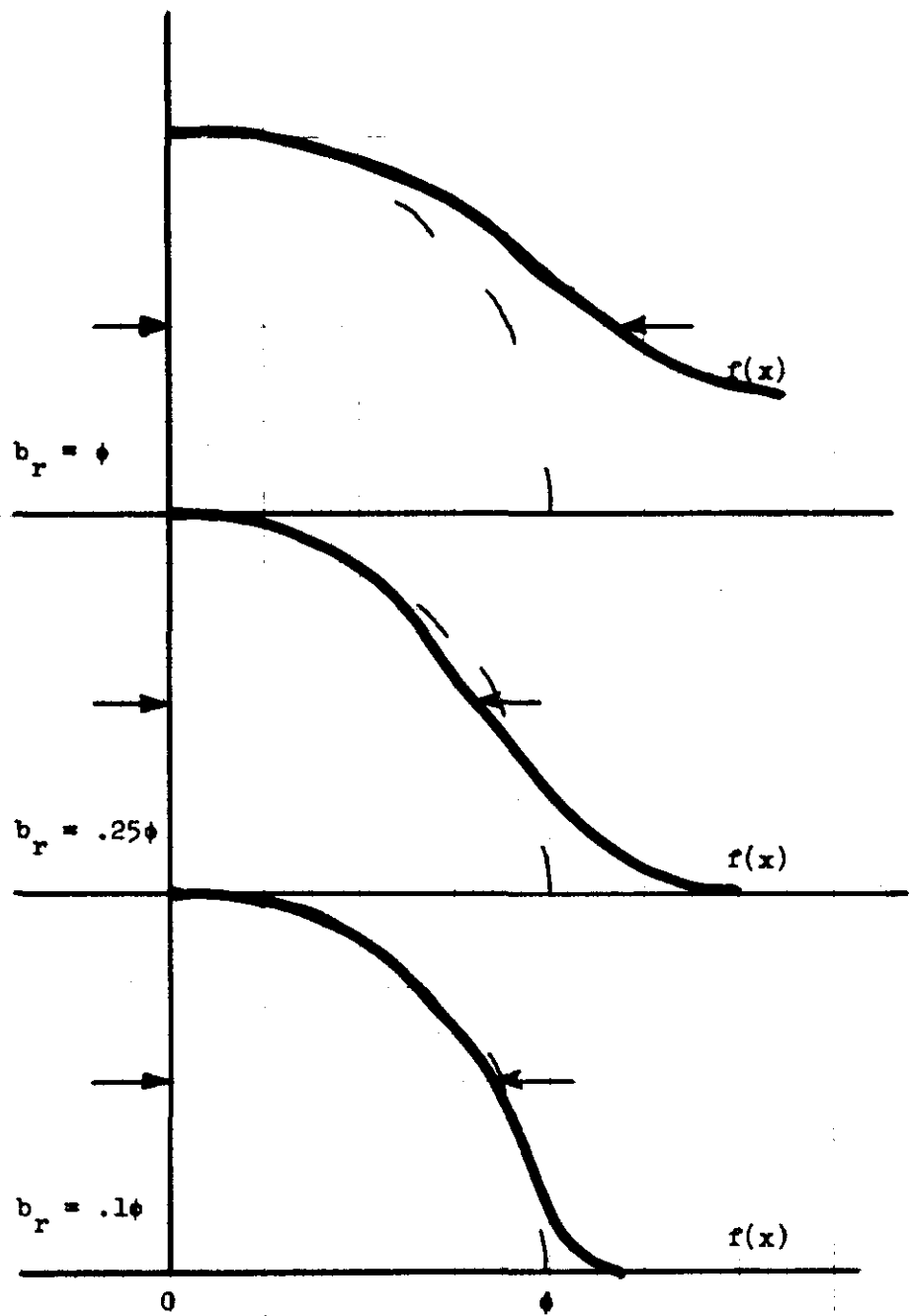


Fig. 5.5,  $--f(x) = g(x)*t(x)$

the observational data presented in this paper (see Table 4.3). However, model restorations for which mean errors are given yield diameters that are still below the true values, mean error notwithstanding. The problem is not resolved. Until it is, one cannot place full reliance on values of angular diameters for small sources as determined by the restoration method. There is no reduction in the worth or accuracy of double star separation measurements as determined from the restoration process.

# VI. Appendix: Model Occultation Curves

Equations (2.1-2.4) define the parameters associated with Fresnel diffraction at a straight edge. The derivation presented here is basically identical with that given by Diercks and Hunger (1952), except that the limb darkening function has been changed.

In binary star studies it is customary to describe the brightness distribution across a stellar disc (Irwin 1962) by

$$J_{\lambda}(\theta) = J_{c,\lambda}(1 - \beta_{\lambda} + \beta_{\lambda} \cos \theta) \quad (\text{A.1})$$

with

$$\begin{aligned} J_{c,\lambda} &= \text{center of disc intensity,} \\ \beta_{\lambda} &= \text{limb darkening coefficient, } 0 \leq \beta_{\lambda} \leq 1, \\ \theta &= \text{angle of surface normal with line of sight.} \end{aligned}$$

Through a coordinate transformation, equation (A.1) can be written as

$$J_{\lambda}(x,y) = J_{c,\lambda}(1 - \beta_{\lambda} + \beta_{\lambda} \sqrt{1-x^2-y^2}) \quad (\text{A.2})$$

with  $x$  and  $y$  as perpendicular coordinate axes mutually perpendicular to the line of sight with  $y$  directed parallel to the diffracting edge. Since no information regarding the brightness distribution in the  $y$ -coordinate can be recovered in a scan along the  $x$ -coordinate, an integration with respect to  $y$  can be done immediately. The total intensity of a strip of width  $dx$  is

$$B_{\lambda}(x)dx = 2 \int_0^{\sqrt{1-x^2}} J_{\lambda}(x,y) dx dy.$$

With the substitution of equation (A.2), the above equation, in normalized form, becomes

$$A(x)dx = \frac{B_{\lambda}(x)dx}{\int B_{\lambda}(x)dx} = \frac{J_{c,\lambda} \{ 2(1-\beta_{\lambda})\sqrt{1-x^2} + (\pi/2)\beta_{\lambda}(1-x^2) \}}{J_{c,\lambda} \pi(1 - 1/3 \beta_{\lambda})} \quad (\text{A.3})$$

The contribution of a single strip of width  $dx$  to the total integrated intensity is  $I(w)A_\lambda(x)dx$ . Thus the total normalized intensity from all strips is

$$\mathcal{J}_\lambda(h_0) = \int_{-1}^{+1} I(w)A_\lambda(x)dx. \quad (A.4)$$

To express  $I(w)$  in terms of  $x$ , a reduced radius  $\rho = \frac{b\phi}{2}$  (where  $\phi$  is the angular diameter) and equation (2.3) are introduced. With these substitutions equation (A.4) becomes

$$\mathcal{J}_\lambda(h_0) = \int_{-1}^{+1} I_\lambda(h_0 + x\rho)A_\lambda(x)dx. \quad (A.5)$$

Unfortunately equation (A.5) cannot be analytically integrated since the implied Fresnel integrals have no closed analytical form. However, the expression in equation (A.5),  $I_\lambda(h_0 + x\rho)$ , can be expanded in a Taylor series about  $h_0$  and integrated term by term. This series is

$$I_\lambda(h_0 + x\rho) = \sum_{n=0}^{\infty} d^n I_\lambda(h_0) \frac{(x\rho)^n}{n!}.$$

After separation of terms and substitution of the above equation, equation (A.5) becomes

$$\mathcal{J}_\lambda(h_0) = \sum_{n=0}^{\infty} \left\{ d^n I_\lambda(h_0) \frac{\rho^n}{n!} \int_{-1}^{+1} x^n A_\lambda(x) dx \right\}. \quad (A.6)$$

But  $\int_{-1}^{+1} A_\lambda(x) dx = 1$  by normalization, and  $A_\lambda(x)$  is an even function. Since for  $n$ -odd  $\int_{-1}^{+1} x^n A_\lambda(x) dx = 0$ , only even-power terms appear, and equation (A.6) is rewritten as

$$\mathcal{J}_\lambda(h_0) = \sum_{n=0}^{\infty} \left\{ d^{2n} I_\lambda(h_0) \frac{\rho^{2n}}{(2n)!} \int_{-1}^{+1} x^{2n} A_\lambda(x) dx \right\}.$$

The  $n^{\text{th}}$  integral, for  $n > 0$ , is given by

$$\int_{-1}^{+1} x^{2n} A_\lambda(x) dx = \frac{1}{2^{n+1}} \left[ \frac{(1 - \beta_\lambda) + \frac{2^{n+2}}{(2n+1)(2n+3)\beta_\lambda}}{1 - 1/3 \beta_\lambda} \right]$$

so that the total intensity due to an extended source in the influence of Fresnel diffraction is

$$I_{\lambda}(h_0) = I_{\lambda}(h_0) + \sum_{n=0}^{\infty} d^{2n} I_{\lambda}(h_0) \frac{\rho^{2n}}{(2n)!} \left( \frac{(1-\beta_{\lambda}) + \frac{2^{n+2}}{(2n+1)(2n+3)\beta_{\lambda}}}{1 - 1/3 \beta_{\lambda}} \right) \quad (A.7)$$

This reduces to  $I_{\lambda}(h_0) = I_{\lambda}(h_0)$  for  $\rho = 0$ , a point source. Only the derivatives of  $I_{\lambda}(h_0)$  need be evaluated to have the complete solution. Given equation (2.1), successive derivatives can be found by applying the chain rule, viz.,

$$\frac{\partial^n I_{\lambda}(h_0)}{\partial h_0^n} = \frac{d^n I(w)}{dw^n} \left( \frac{\partial w}{\partial h_0} \right)^n \quad \text{where} \quad \frac{\partial w}{\partial h_0} = \sqrt{\frac{2}{\lambda b}}.$$

The derivatives of  $I(w)$ ,  $d^n I/dw^n$ , are easily found, the first few of them being

$$\begin{aligned} I' &= (1/2 + C(w)) \cos \frac{\pi w^2}{2} + (1/2 + S(w)) \sin \frac{\pi w^2}{2} \\ I'' &= 1 + \pi w \left\{ (1/2 + S(w)) \cos \frac{\pi w^2}{2} - (1/2 + C(w)) \sin \frac{\pi w^2}{2} \right\} \\ I''' &= -3\pi^2 w I' - \pi^2 w^2 I'' \end{aligned}$$

The Fresnel functions,  $C(w)$  and  $S(w)$ , are evaluated with series expansions given by Lotsch (1964).

Using equation (A.7), or its numerical integration counterpart equation (2.7), model occultation curves have been generated with the following parameters:  $\lambda = 4.7 \times 10^{-7}$  meters,  $b = 3.792 \times 10^8$  meters,  $v_r = -.3500$  "/second, and  $\tau = .00104$  seconds. Figures A.1 and A.2 illustrate the models qualitatively. Each curve is plotted as normalized intensity vs. time.

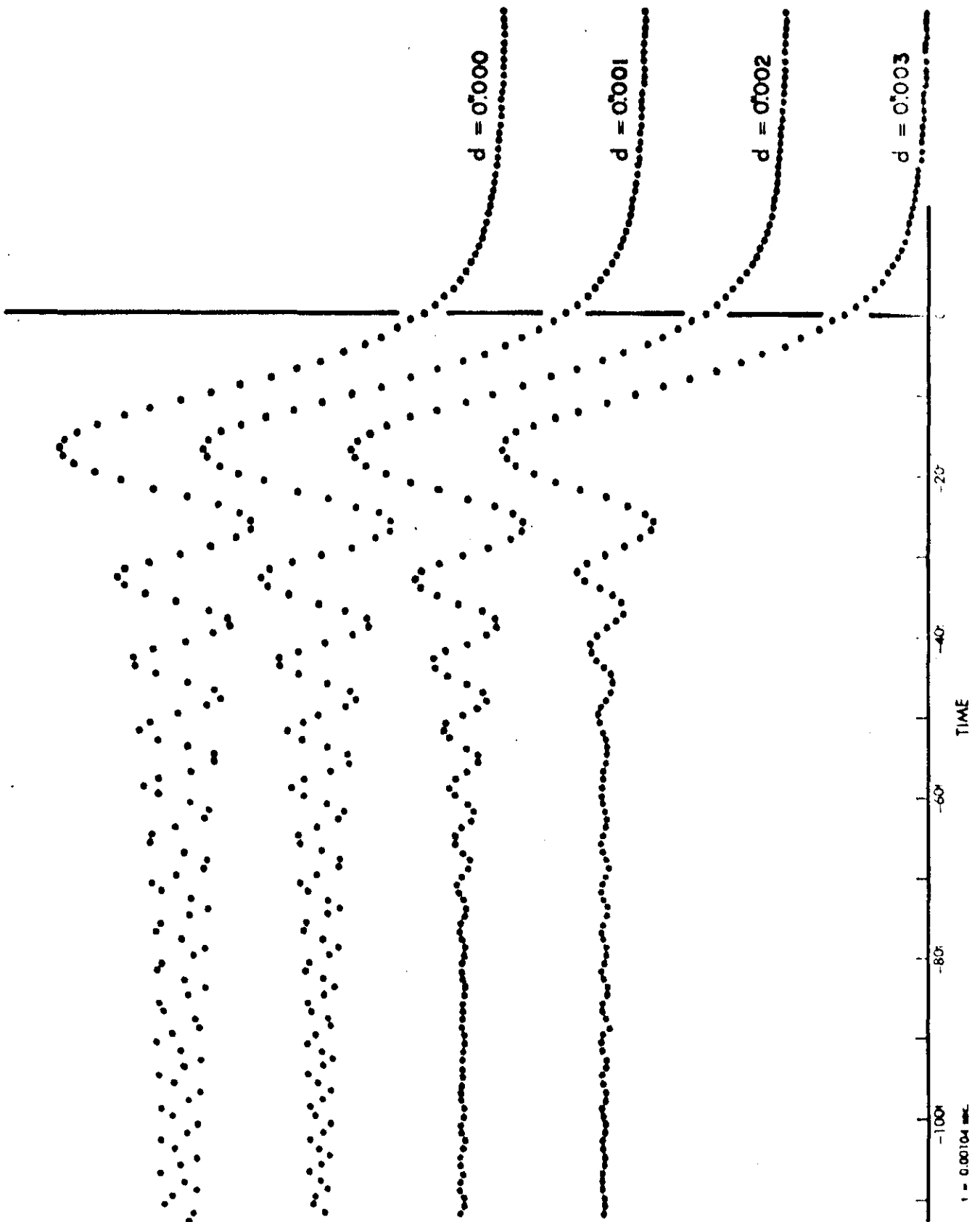


FIGURE A.1.--Model Occultation Curves

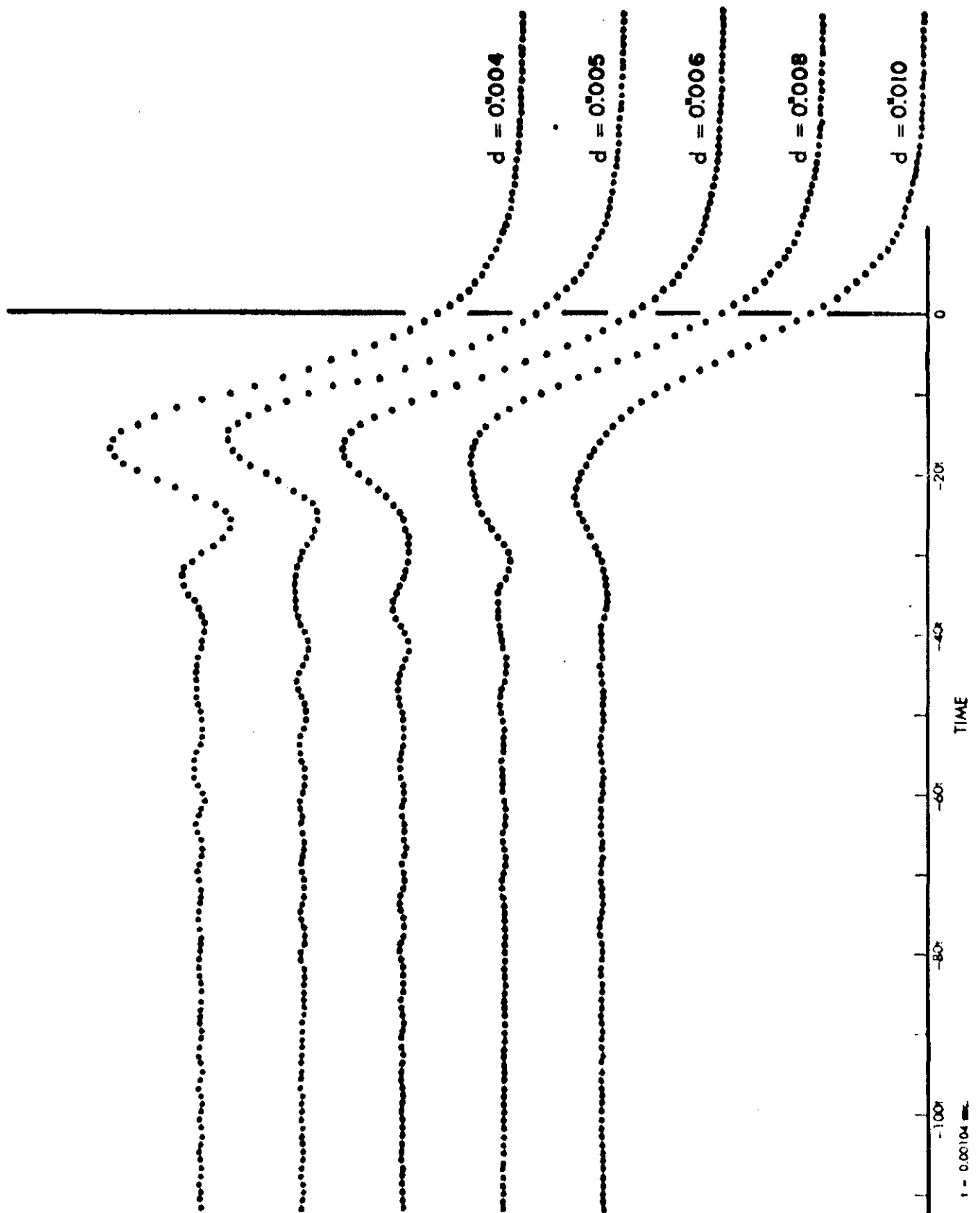


FIGURE A.2.--Model Occultation Curves.



## VII. References

- Abt, H.A., Barnes, R.C., Biggs, E.S., and Osmer, P.S. 1965, Ap. J., 142, 1604.
- Allen, C.W. 1963, Astrophysical Quantities (2nd ed.; London: Athlone Press).
- Aller, L.H. 1963, Astrophysics: The Atmospheres of the Sun and Stars (New York: Ronald Press).
- Berg, R.A. 1967, Publ. Leander McCormick Obs., XV, part IV, 19.
- Binnendijk, L. 1960, Properties of Double Stars (Philadelphia: University of Pennsylvania Press), pp. 74 ff.
- Birney, D.S. 1966, Sky and Telescope, 31, 210.
- Born, M. and Wolf, E. 1964, Principles of Optics (4th ed.; London: Pergamon Press).
- Bracewell, R.N. 1956, Australian J. Phys., 9, 198.
- Brown, R.H. 1968a, Nature, 218, 637.
- 1968b, Ann. Rev. Astron. and Ap., 6 (Palo Alto, Calif.: Annual Reviews, Inc.), pp. 13-38.
- Brown, R.H., Davis, J., and Allen, L. 1967, M.N.R.A.S., 137, 375.
- Code, A.D., and Liller, W.C. 1962, in Astronomical Techniques, ed. W.A. Hiltner (Chicago: University of Chicago Press), pg. 284.
- Cousins, A.W.J., and Guelke, R. 1953, M.N.R.A.S., 113, 776.
- Diercks, H., and Hunger, K. 1952, Zs. f. Ap., 31, 182.
- Doremus, C. 1968 (private communication).
- Dunham, D.W. 1969 (private communication).
- Eddington, A.S. 1909, M.N.R.A.S., 69, 178.
- Evans, D.S. 1951, M.N.R.A.S., 111, 64.
- 1955, ibid., 115, 466.
- 1957, A. J., 62, 83.
- Evans, D.S., Heydenrych, J.C.R., and van Wyk, D.N. 1953, M.N.R.A.S., 113, 781.
- Gray, D.F. 1967, Ap. J., 149, 317.
- Herr, R.B. 1969, Publ. A. S. P., 81, 105.

- Hertzsprung, E. 1947, Ann. Leiden Obs., 19, part 16, 93.
- Irwin, J. 1962, in Astronomical Techniques, ed. W.A. Hiltner (Chicago: University of Chicago Press), p. 588.
- Johnson, H.L., and Mitchell, R.I. 1958, Ap. J., 128, 31.
- Johnson, H.M. 1968, in Nebulae and Interstellar Matter, eds. B.M. Middlehurst and L.H. Aller (Chicago: University of Chicago Press), pg. 78.
- Lotsch, H. 1964, Comm. A. C. M., 7, 660.
- McMahon, P.A. 1908, M.N.R.A.S., 69, 126.
- Mendoza, E.E. 1956, Ap. J., 123, 54.
- Michelson, A.A. 1920, Ap. J., 51, 257.
- Michelson, A.A., and Pease, F.G. 1921, Ap. J., 53, 249.
- Morton, D.C., and Adams, T.F. 1968, Ap. J., 151, 614.
- Nather, R.E. 1969 (private communication).
- Pease, F.G. 1930, Scientific American, 143, 290.
- Rakos, K.D. 1964, A. J., 69, 556(A).
- 1967, "Die Bestimmung von Sterndurchmessern mit Hilfe der Verzerrung der Fresnelschen Beugungsfigur bei der Bedeckung durch den Mond," (unpublished).
- Scheuer, P.A.G. 1962, Australian J. Phys., 15, 333.
- Smirnov, N.V. 1965, Tables of the Normal Probability Integral, the Normal Density, and Its Normalized Derivative (New York: The Macmillan Company).
- Smith, B., and Struve, O. 1944, Ap. J., 100, 360.
- Taylor, J.H. 1966, Nature, 210, 1105.
- van Flandern, T.C. 1965, Sky and Telescope, 29, 386.
- von Hoerner, S. 1964, Ap. J., 140, 65.
- 1965, ibid., 142, 1265.
- Watts, C.B. 1963, "The Marginal Zone of the Moon," A.P.A.E., 17.
- Whitford, A.E. 1939, Ap. J., 89, 472.
- Williams, J.D. 1939, Ap. J., 89, 467.
- Wood, H.J., and Lockwood, G.W. 1967, Publ. Leander McCormick Obs., XV, part IV, 25.

## VIII. Acknowledgments

It is with pleasure that I express my thanks to the faculty and staff at McCormick Observatory who have made my dissertation research both fruitful and enjoyable. Special measures of gratitude go to my advisor, Dr. H. John Wood, for continued discussions, constructive criticisms, and observational assistance during all phases of the work, to Mr. Robert P. Redick, the Observatory's electronic engineer, who provided the technical skills needed during the designing and testing of the photon counter, and to Mr. Charles Smith for his assistance at the telescope.

Thanks are due the United States Air Force Aeronautical Chart and Information Center, St. Louis, Missouri, for financially supporting me, the University of Virginia Computing Science Center whose grant enabled me to implement the analytical reduction program, the National Science Foundation whose grants GP 7467 and GP 8990 to Dr. Wood constructed the pulse counter and made travel to Kitt Peak National Observatory possible, and the U.S. Naval Observatory for providing precise occultation predictions.

My greatest thanks go to my wife, Rebecca Myers Berg, for her loving kindness, moral support, and professional criticisms.

